LIMITATIONS OF PASSIVE THERMAL MANAGEMENT FOR A-LINE SOLID STATE LIGHTING TECHNOLOGIES

A Master of Science Thesis

by

Muhammed Nasır İnan

Submitted to the
Graduate School of Engineering
In Partial Fulfillment of the Requirements for the Degree of

Master of Science

in the
Department of Mechanical Engineering

Özyeğin University
January 2015

LIMITATIONS OF PASSIVE THERMAL MANAGEMENT FOR A-LINE SOLID STATE LIGHTING TECHNOLOGIES

Approved by:

Associate Professor Mehmet Arık, Advisor
Department of Mechanical Engineering
Özyeğin University

Assistant Professor Sedat Nizamoğlu
Department of Electrical and Electronics Engineering
Özyeğin University

Assistant Professor Altuğ Başol
Department of Mechanical Engineering
Özyeğin University

Date Approved: 12 January 2015

ABSTRACT

Energy has been one of the most important problems for the last few decades. Efficient use of energy is as important as efficiency in energy production and transportation. Solid state lighting (SSL) technology may reduce consumed energy in buildings from 20 percent to less than 5 percent. Light emitting diodes (LEDs) have recently been evolved as a novel lighting technology that is over 7-10 times more efficient than conventional-old incandescent lamps. Although LED lighting systems have many other advantages as being more reliable and having longer lifetimes than conventional energy lighting systems like environmentally hazardous fluorescent lamps, they are based on solid state technology with thermal limitations. Low junction temperature requirement is one of the most important challenges for the high luminosity LED lighting systems, which also have high heat generation rates. Junction temperature of LEDs is directly related with reliability, lifetime, light output and quality. Therefore, thermal management is crucial for LED lighting systems.

Passive thermal management of LED lighting systems has many advantages as simplicity, reliability, low cost and silent operation. Nevertheless, high cooling capacity requirement means large passive cooling components, which push the limits of the form factor standards. Besides the size and weight limitations, tight interaction between thermal management and optical design obligate researchers to develop all components in a compact system. In this study, different passive thermal management systems for high luminosity A-line LED lamps are investigated. Commercial A-line LED bulbs with various passive cooling approaches and designs are experimentally studied in order to bring thermal, optical and dimensional limitations into view.

A new system level passive thermal management approach based on buoyancy driven chimney effect is computationally developed. The optical design of the system is also

computationally developed at the same time. All computational results are validated with the experimental results. Computational and experimental results of the developed and manufactured system are analyzed, and the system is computationally optimized. Finally, several figure of merits (FOMs) are developed for SSL systems for the advancement of science and technology. Thus, various commercially available bulbs and developed prototypes are compared to bring various design options into view.

ÖZETÇE

Enerji son bir kaç on yıldır en önemli problemlerden biri olmuştur. Enerjinin verimli kullanılması enerjinin üretimindeki ve taşınmasındaki verimlilik kadar önemlidir. Katı hal aydınlatma (SSL) teknolojisi binalarda tüketilen enerjiyi yüzde 20'den yüzde 5'ten daha aşağıya düşürebilir. Geleneksel akkor lambalardan 7-10 kere daha verimli olan ışık yayan diyotlar (LED) son dönemde özgün bir aydınlatma teknolojisi olarak gelişti. LED aydınlatma sistemleri, çevreye zararlı floresan lambalar gibi geleneksel aydınlatma sistemlerine nazaran daha güvenilir olma ve daha uzun kullanım ömrüne sahip olma gibi avantajlara sahip olsa da, termal limitleri olan katı hal teknolojisine dayanırlar. Düşük jonksiyon sıcaklığı ihtiyacı yüksek aydınlatma gücüne ve ısı üretimine sahip LED aydınlatma sistemleri için en büyük problemlerden biridir. LED'lerin jonksiyon sıcaklığı, güvenilirlik, kullanım ömrü, ışık çıkışı ve ışık kalitesi ile doğrudan ilgilidir. Bu yüzden, ısıl yönetim LED aydınlatma sistemleri için çok önemlidir.

LED aydınlatma sistemlerinin pasif ısıl yönetimi basitlik, güvenilirlik, düşük maliyet ve sessiz çalışma gibi avantajlara sahiptir. Buna rağmen yüksek soğutma kapasitesi ihtiyacı, form faktör standartlarının sınırlarını zorlayan büyük pasif soğutma komponentleri anlamına gelmektedir. Boyut ve ağırlık limitlerinin yanında, ısıl yönetim ve optik dizayn arasındaki sıkı etkileşim araştırmacıları bütün komponentleri kompakt bir sistem olarak birlikte geliştirmeye mecbur etmektedir. Bu çalışmada, yüksek ışık gücüne sahip standart A serisi LED lambaları için olan farklı pasif ısıl yönetim sistemleri araştırılmaktadır. Çeşitli pasif soğutma yaklaşımlarına ve tasarımlarına sahip ticari A serisi LED lambalar boyutsal, termal ve optik limitleri ortaya çıkarmak için deneysel olarak çalışılmaktadır.

Boyansi ile çalışan baca etkisine dayanan sistem seviyesindeki yeni bir ısıl yönetim yaklaşımı sayısal olarak geliştirilmiştir. Sistemin optik dizaynı da aynı zamanda sayısal olarak geliştirilmiştir. Bütün sayısal sonuçlar deneysel sonuçlarla doğrulanmıştır.

Geliştirilen ve üretilen sistemin sayısal ve deneysel sonuçları analiz edilmiştir ve sayısal olarak optimize edilmiştir. Son olarak, bilim ve teknolojinin ilerlemesine katkı sağlayacak SSL sistemleri için çeşitli başarım ölçüleri (FOM) geliştirilmiştir. Böylece ticari olarak temin edilebilir çeşitli lambalar ve geliştirilen prototipler karşılaştırılarak çeşitli tasarım seçenekleri gözler önüne serilmiştir.

ACKNOWLEDGEMENTS

I am greatly indebted to my thesis supervisor Associate Professor Dr. Mehmet Arık for providing me professional guidance, constant encouragement and moral support from the beginning of the work during study period. I am also thankful to him for giving me opportunity to find my own direction rather than giving me a definite direction. I am also greatly indebted to Assistant Professor Sedat Nizamoğlu and Assistant Professor Altuğ Başol for their valuable support and suggestions to accomplish the study.

I thank for the project support of Istanbul Development Agency and EU FP7 CIG. I am also grateful for the days that I spent for doing research in EVATEG research center at Özyeğin University and to all the colleagues in ARTgroup. Friendships and days spent with my colleagues and Dr. Arık are incomparable and unforgettable!

TABLE OF CONTENTS

LIST OF TABLES

LIST OF FIGURES

LIST OF EQUATIONS

NOMENCLATURE

A	Heat transfer area (m^2)
A_{hs}	Heat sink surface area (m^2)
A_s	Surface area (m^2)
ANSI	American National Standards Institute
CCT	Correlated color temperature (K)
CRI	Color rendering index
Cu	Copper
FR	Flame Retardant
FVM	Finite-volume methods
h	Convection heat transfer coefficient (W/m2-K)
IR	Infrared
k	Thermal conductivity
LPW	Luminious efficacy (lm/W)
l_f	Fin length (mm)
MCPCB	Metal core printed circuit board
m_{hs}	Heat sink weight (g)
LED	Light Emitting Diode

P	Input power (W)
PCB	Printed circuit board
PHS	Passive heat spreader
PMMA	Poly (methyl methacrylate)
PPS	Polyphenylene sulfide
Q	Heat flow rate (W)
R	Thermal resistance (°C/W)
RTV	Room temperature vulcanization
T_a	Ambient temperature (K)
T_{max}	Highest temperature (°C)
t_b	Heat sink base thickness (μm)
t_f	Fin thickness (μm)
T_{hs_max}	Maximum heat sink temperature (°C)
T_{hs_mean}	Mean heat sink temperature (°C)
T_{hs_min}	Minimum heat sink temperature (°C)
TPG	Thermal pyrolytic graphite
T_s	Surface temperature (K)
T_{surr}	Surrounding surface temperature (K)
T_{water}	Water temperature (°C)

ΔT	Temperature difference (°C)
Δx	Thickness of layer (m)
ε	Surface emissivity
σ	Stefan-Boltzmann constant ($5.67\text{-}10^{-8}$ W/m^{-2}-K^{-4})
Φ	Luminous flux (lm)
Φ_e	Radiant flux (W)

CHAPTER I

INTRODUCTION

1.1 LED Lighting Systems

An LED (Light Emitting Diode) is a semiconductor, which is used by various illumination concepts from indicator lamps to street lamps. LED lighting systems can be 5-7 times more efficient than conventional lighting systems. High reliability and long lifetimes over 50000 hours are other facts, which make LED lightings systems advantageous. An LED lighting system contains many components with various purposes. LED packages, optical components, diffuser, thermal interface material (TIM), printed circuit board (PCB), heat sink, electronic driver circuit, isolation, and screw-in (Edison) base are the main components as shown in Figure 1.

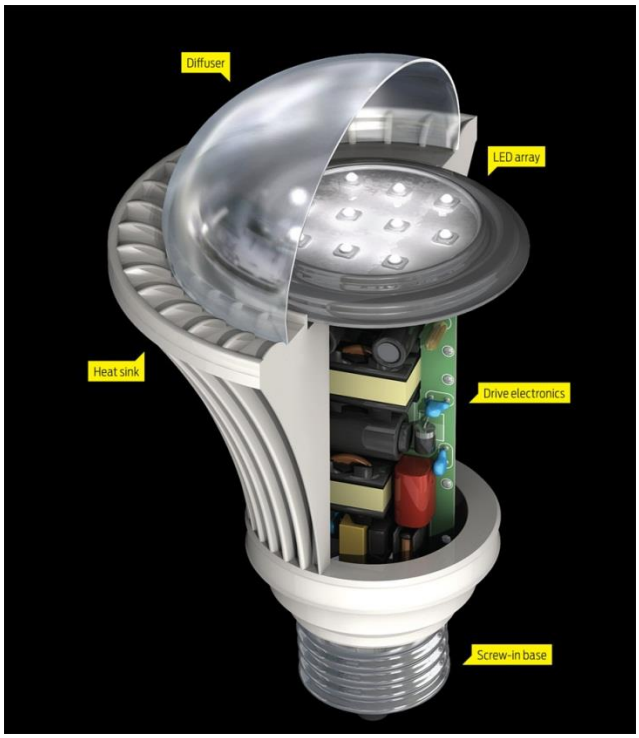

Figure 1: A typical LED lighting system with various components [1]

CHAPTER I

All components of the system are developed mainly based on the functionality and the reliability of the light generating LED chips. LED chips cannot be assembled independently in a system because of its electrical, optical, thermal and mechanical requirements. Therefore, the design and the operation of an SSL lamp is cross-functional. LED packages are electrically connected with electrical driver circuit and isolated from other components by a PCB. PCB is also the thermal connection between LED packages and heat sink and spreads heat to a large area on heat sink base.

TIMs are used for enhancing the heat transfer between two solid components like PCB and heat sink. These materials are used to fill the gaps between solid surfaces due to their roughness. High reflectivity for visible light is also an important property for PCBs. Heat sink is the cooling component with high heat removal capacity. Electronic driver circuit converts the high voltage alternating current to a low voltage direct current for driving LEDs. Isolation component isolates heat sink from Edison base electrically. Edison base is the electrical connection of the system with network. Diffuser protects LEDs, and it guides and diffuses the generated light by LEDs. Some diffusers have phosphor layers for the light conversion that is called remote phosphor application. Some of the LED systems use reflectors to guide the light stronger and decrease the absorption for visible light. There are various LED lighting systems due to their operational areas and conditions. Some of the most popular LED lamps are shown in Figure 2, and they are named as A21, MR16, and PAR38 lamps.

CHAPTER I

Figure 2: Various LED lighting systems [2, 3, 4]

1.2 A-line LED Lamps

A-line LED lamps have standard household incandescent light bulb shape. Most commonly used A-line lamps are A19-A21 bulbs, which have an E26 screw base. “E” means Edison and “26” indicates the wideness of it in mm. American National Standards Institute (ANSI) represents the geometrical standards of an A19 bulb as seen in Figure 3.

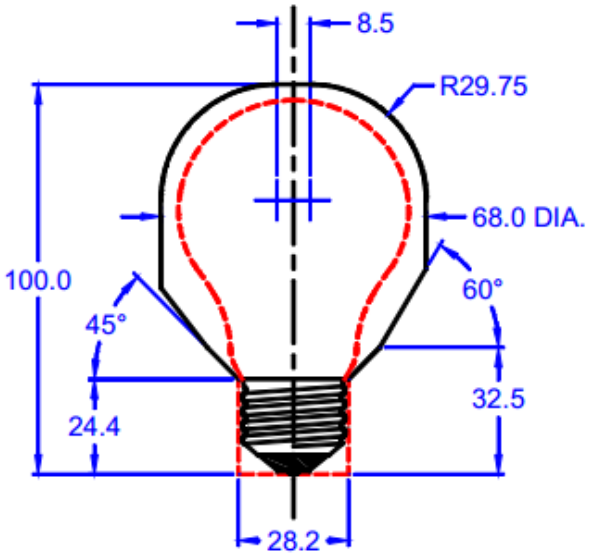

Figure 3: A19 dimension (in mm) [5]

A-line LED bulbs are also classified based on their luminous intensity distributions. While some lamps have more forward intensity distribution, the ones with omni-directional intensity distributions are widely used. Homogeneous intensity for the 4π geometry is an important requirement for these bulbs.

1.3 Heat Transfer Basics and Thermal Management of LED Lighting Systems

Increasing functionality of electronic devices brings high input power requirements and heat generation rates on electronic components. High heat fluxes on compact electronics require proper thermal management, in order to maintain the operating temperature at a safe value for keeping its functionality. It is not always adequate to enhance the efficiency not to face thermal issues, although it is the primary method. When the efficiency of an electronic device has a limited scope for the further improvement, an adequate way of heat removal should be considered as well. In the recent decades, thermal management of the electronic devices is considered in the design phase and some of them are designed as a complete system with thermal management components.

LEDs and electronic driver circuits are the heat-generating components of LED lighting systems. Heat should be removed from these heat-generating components with a proper thermal management. Heat removal starts with the conduction from LED chips or electronic components to the surface of cooling components. Fourier's law of conduction (Equation 1) expresses the rate of heat conduction through a plane is given as;

$$\dot{Q}_{cond} = -kA\frac{\Delta T}{\Delta x} \tag{1}$$

CHAPTER I

Fourier's law indicates that thermal path between heat sources and cooling components should be as short as possible, with the highest thermal conductivity and largest heat transfer area to decrease the temperature of the heat source for the same heat flow rate and ambient temperature. Since the components between LEDs and the cooling components have also electrical, mechanical, weight and optical requirements, it is not a simple task to meet them all at the same time. High rate of heat conduction is required mainly between the heat sources (LEDs and electronic components) and the cooling components such as heat sink. Even when the heat is conducted to other components effectively, their poor cooling capacities downplay the low temperature difference between heat source and component.

After heat is transferred to the surface of an LED lighting system exposed to ambient air, it is removed to air with natural convection and thermal radiation. The rate of convection heat transfer (2) is expressed by Newton's law of cooling as;

$$\dot{Q}_{conv} = hA_s(T_s - T_a) \tag{2}$$

The rate of radiation heat transfer (3) between two surfaces is given by Stefan-Boltzmann law as;

$$\dot{Q}_{rad} = \varepsilon\sigma A_s(T_s^4 - T_{surr}^4) \tag{3}$$

Large surface area is indispensable for passive cooling components, since it has a large scope for increment, and the surface area can be also expanded based on surface properties. The method for increasing the surface temperature for the same heat flow rate is an effective conduction heat transfer from the heat sources to the external surfaces. Heat transfer coefficient is mainly based on the heat sink geometry in interaction with other components that affects natural convection development. Heat transfer coefficient of a heat sink can be increased by optimization for the same

dimensions. The resistance of a heat sink to fluid should be as low as possible whereby the heat should be transferred to flowing air as much as possible. These two requirements can conflict with each other for many cooling components such as a passively cooled finned-heat sink. Since all of the mentioned parameters are in interaction with each other, the complex optimization task should be well studied.

1.4 Opto-thermal Chimney Approach for High Power LED Lamps

The demand for SSL systems with high light outputs lead to significant heat generation rates, which increase the junction temperature on LED chips. Moreover, the changes on the junction temperature strictly affect the reliability, lifetime, light quality and luminous flux. Because of their simplicity, reliability, low cost and silent operation, passive cooling systems are preferred for the thermal management of LED lighting systems.

Heat sink is the main cooling component of an LED lighting system such as a typical A-line LED bulb. Heat is dissipated from finned surfaces to ambient air with primarily natural convection and partially thermal radiation. High flow rates of high-luminosity LED lamps require large surface areas, which push the limits of the form factors. Increasing the heat removal capacity is possible by the optimization of a heat sink, which provides the effective use of the reserved volume. Using chimney effect is an effective method for passive thermal management, and it is already used for extending the limits of passive thermal management of electronics. On the other hand, optimization and effective utilization of a heat sink is limited by the optical requirements of A-line LED bulbs. Since omni-directional and homogenous luminous intensity distribution requirement of an optical design is also taking its shape based on thermal management components. Therefore, thermal management and optical design

approach should be considered carefully by regarding the tight interaction between them.

1.5 Objectives and Organization of the Study

This thesis investigates thermal, optical and dimensional limitations of passively cooled A-line SSL systems. A new approach based on chimney effect is proposed for a combination of advanced system level thermal management, optical design and light-weight for A-line SSL technologies. System level opto-thermal analysis and evaluation of existing approaches and newly developed approach are objectives of this study as well.

This thesis consists of six chapters. Thermal and optical requirements of LED lighting systems, opto-thermal chimney approach for LED lighting systems and the scope of the present study is outlined in the first chapter. Chapter 2 presents the literature review of the theoretical, computational and experimental studies on thermal management of LED lighting systems, chimney effect on natural convection cooling and computational methods in heat transfer and optics. The experimental results of existing A-line LED lighting systems are presented in Chapter 3. Chapter 4 includes the development of new concept, computational and experimental studies for new approach and computational optimization of the prototype of new approach. The following chapter presents the figure of merits for SSL systems for analysis and evaluation of existing and newly developed passive cooling approaches for A-line SSL systems. The contribution of this research and recommendation for future work is summarized in Chapter 6.

CHAPTER II

LITERATURE REVIEW

2.1 Thermal Management of LED Lighting Systems

Thermal management of LED lightings systems is studied in different levels from package to system. Most of heat is conducted through the multiple metallic/non-metallic parts of the package to heat sink and finally dissipated to ambient environment as illustrated in Figure 4 [6].

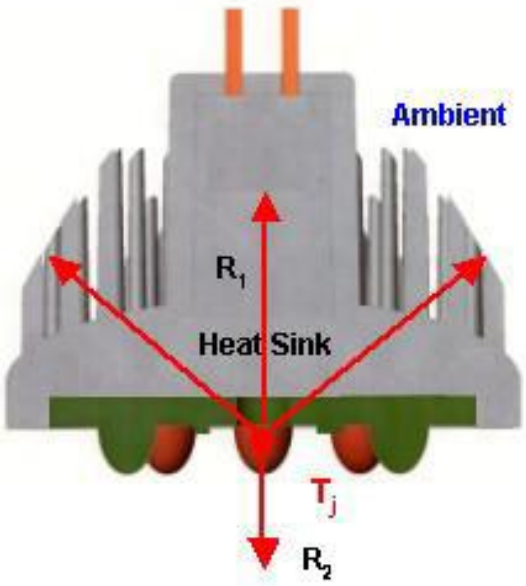

Figure 4: Heat transfer by a typical LED illumination system [6]

Heat transfer bottleneck at any levels on the thermal path limits the performance at any other levels. Therefore, thermal management in all levels should be enhanced, whereby the enhancement of the bottleneck has a particular significance that ensures the maximum utilization of total heat transfer capacity.

CHAPTER II

2.1.1 Package Level Thermal Management

A LED chip consisting of p-n junctions is created with doped semiconducting materials that are packaged for meeting the operational requirements and keeping the functionality. The schematic of a typical LED package composed of several components can be seen in Figure 5. An LED die is attached to a heat slug with a die attach material, which provides the electrical isolation with the rest of the system and thermal connection with heat slug. LED die is connected to an electrical source over bonding wires and a lead frame. The encapsulant consisting of dispersed phosphors protects the LED die and guides the emitted light. Phosphors absorb some part of the emitted light dominantly in the electromagnetic wavelength range of blue light and emit white light, whereby some part of the energy is converted into heat.

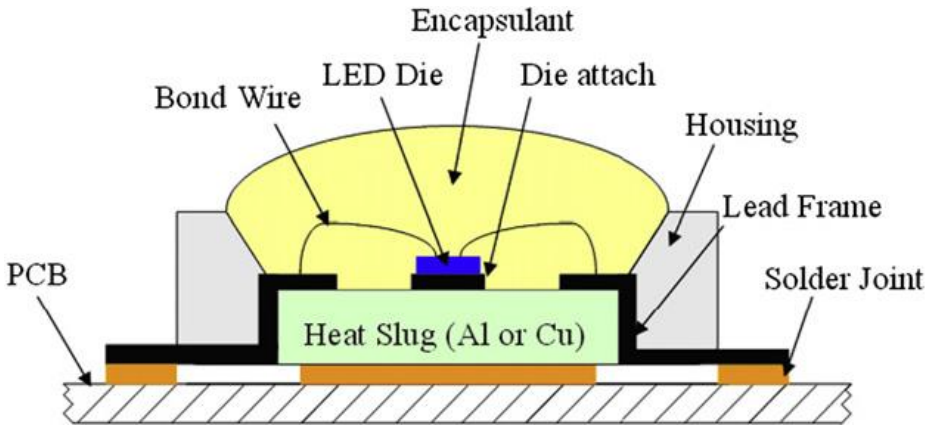

Figure 5: LED package structure [7]

Heat transfer between an LED die and a PCB is limited due to the limited heat conduction path. Thermal path between an LED chip and a board is shown in Figure 6. Thermal resistance on the thermal path shows how many Celsius degrees junction temperature rises for each Watt of electrical power.

CHAPTER II

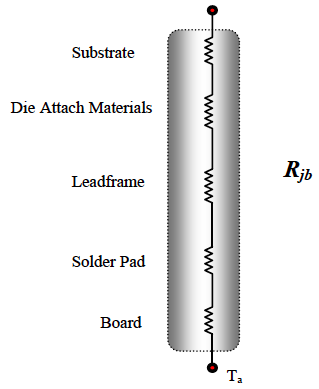

Figure 6: Simplified thermal resistance network of an LED package [8]

You et al. studied on die attach material, which has the lowest thermal conductivity compared to other packaging materials and limited heat transfer area [8]. Several die attach materials from several suppliers are tested experimentally in order to observe the effect of the thermal conductivity on the thermal performance. Tested die attach materials showed different thermal conductivities between 1.2 W/m-K and 60 W/m-K. Figure 7 shows the temperature difference between junction and board for a 1 W-blue LED with dominate wavelength of 460 nm.

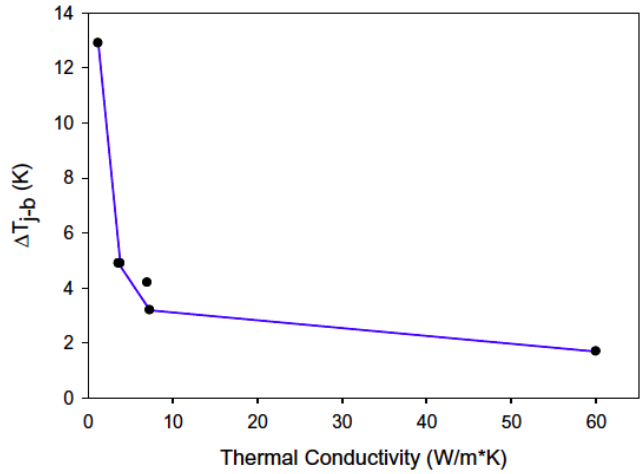

Figure 7: Temperature difference between junction and for various thermal conductivities [8]

As seen in Figure 7, it was achieved to reduce the temperature difference considerably by using a high conductive die attach material. This study also shows that the highest impact of the thermal conductivity seen for smaller thermal conductivities than approximately 5 W/m-K. Thermal resistance of 12.9 K/W of the package consisting of a die attach material with a thermal conductivity of 1.2 W/m-K was reduced to 1.7 W/m-K through an advanced die attach material with a thermal conductivity of 60 W/m-K. This is a high thermal conductivity for a die attach material but the thermal resistance was still reduced to 3.2 K/W with a thermal conductivity of 7.3 W/m-K.

Once the thermal bottleneck of a component in an SSL lighting system is removed, heat transfer capacity of other components on the thermal path is better utilized. By the further improvement of thermal performance of the components, thermal management of the package is becoming a matter of the limitations of the other components. The design of an LED package is a complex task including the reliability parameters. Thermo-mechanical properties of the components in an LED package should be identical so that reliability issues and thermal bottlenecks due to degradations are not faced.

2.1.2 Board Level Thermal Management

Board level thermal management is basically the starting point of a system level thermal management, since it limits the transfer of heat to cooling component. It is crucial that each system has its own board level thermal design that responds to its requirements.

One study [9] investigated the effects of spacing of LED packages on a metal core printed circuit board (MCPCB). As shown in Figure 8, spacing is the primary factor for tightly aligned high power (1-Watt class for this study) LED arrays on a MCPCB

until the spacing reaches approximately 3 mm. When an LED reaches a diameter of 4-5 mm spacing, intersection of heating zones is limited, and this fact reduces its effect on the thermal resistance significantly. Thinner solder layers, thicker copper layers and thinner dielectric layers were secondary factors in this study, which reduced the thermal resistance. This study indicates that an LED array with an adequate spacing can significantly enhance the thermal performance.

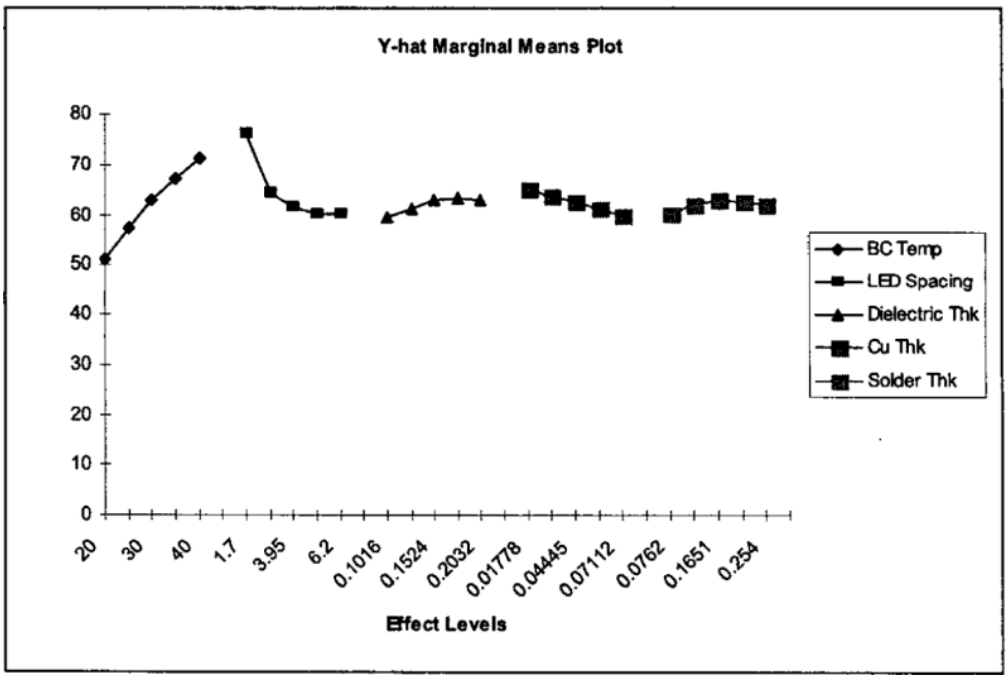

Figure 8: Plot for various parameters on LED system temperatures [9]

Another study [10] that investigated PCB based thermo-syphon concept, which eliminates extra thermal interface material (TIM) as well as the necessity of an electrical insulation layer between heat sink and PCB, showed the critical role of PCB layers creating bottlenecks on thermal path to heat sink. Figure 9 illustrates the cross-sectional representation of passive heat spreader (PHS) PCB with a single LED package attached to a copper evaporator.

CHAPTER II

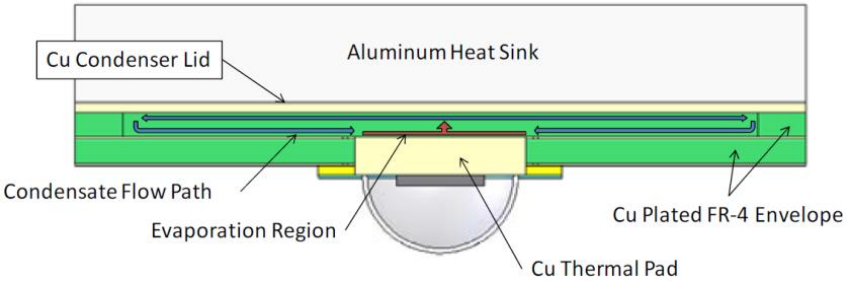

Figure 9: Cross-sectional depiction of the PHS PCB [10]

The dielectric fluid over the PCB is vaporized by an evaporator, subsequently condensed back to liquid by the Cu condenser lid attached to heat sink and falls back to the evaporator. PHS, FR-4 and metal core PCBs with high brightness LEDs were analyzed using a commercial CFD Software. The configurations of PCBs are shown in Table 1, Table 2 and Table 3. The thermal resistances were respectively 26.6 °C/W, 7.2 °C/W and 3.7 °C/W for FR-4, metal core and PHS PCBs based on the computational results, which show the explicit role of various PCB layers.

Table 1: FR-4 PCB configuration [10]

Component	Thickness (μm)	Thermal conductivity (W/m-K)
Top layer copper	70	398
FR-4	1588	0.2
Filled via (SnAgCu)	1588	59
Bottom layer copper	70	398
Total	1728	-

Table 2: Metal core PCB configuration [10]

Component	Thickness (μm)	Thermal conductivity (W/m-K)
Top layer copper	70	398
PCB dielectric	100	2.2
Al plate	1588	150
Total	1758	-

Table 3: PHS PCB configuration [10]

Component	Thickness (μm)	Thermal conductivity (W/m-K)	Heat transfer coefficient (W/m^2-K)
Copper plug (area 3.3 x 1.65 mm)	728	398	-
Top layer copper	70	398	-
FR-4 dielectric	588	0.2	-
Bottom layer copper	70	398	-
Evaporator copper	-	-	20000
Vapor space	600	100000	-
Condenser surface	-	-	10000
Copper chamber	1000	398	-
Total	1728	-	-

2.1.3 System Level Thermal Management

Package and board level thermal management aim an effective heat transfer between the junction and the cooling component of the system. Implementation of advanced thermal materials and advanced mounting technologies can standalone enhance the thermal performance in this area, when production and cost parameters are at allowable levels. System level thermal management is a matter of heat removal to air with convection and thermal radiation besides the conduction heat transfer. This makes the solution of the thermal problem challenging within the limitations of natural convection cooling because of the size and weight limitations of the system. On the other hand, implementation of a forced cooling component brings several problems such as high cost, high complexity, low reliability and noise. For this reason, forced cooling components are not preferred due to the operational conditions and requirements of SSL lighting systems.

Inan and Arik [11] emphasized that metal based heat sinks are widely used passive

cooling components for the last few decades since the cooling of electronics started to become a major challenge for engineers. Because of their simplicity, reliability, low cost and silent operation, passive metal based heat sinks are still preferred as the main cooling components of typical LED lamps for both LEDs and drive electronics. Besides the simplicity of fabrication without the requirement of a high-tech manufacturing facility, mature industrial utilities keep heat sink production low priced on this long-experienced field. This was also driven by the electronics industry while the performance has been increasing; and the size and cost has been shrinking.

Complex task of a heat sink design includes also the aesthetic side like thermal, optical and mechanical aspects. Heat sink requirements are changing by the cooling needs of different electronics with various size, weight and operational standards. Heat sinks used in LED lamps do not only cool the system but also help to assemble thermal, electronic and optical components. Heat is dissipated dominantly from finned surfaces to ambient air with primarily natural convection and partially thermal radiation. But a large surface area and a large weight are required, which conflict with the limitations of the standardized lamps. Thus, the optimization of the heat sink in an LED system is crucial. There are a number of studies about the heat sink optimization attempted to address this need.

Table 4: Range of geometric parameters [12]

Parameter	Minimum value (mm)	Maximum value (mm)	Incremental value
Fin height	8	18	5
Fin thickness	1	3	1
Base thickness	2	4	1
Fin Pitch	3	5	1

CHAPTER II

Alvin et al. [12] has numerically investigated the optimization of the heat sink parameters like fin height, fin thickness, fin pitch and base height in given ranges (Table 4) for the cooling of a 10 W LED lamp. The results of CFD analyses are given in Table 5.

Table 5: Simulation results [12]

Fin height (mm)	Fin thickness (mm)	Fin number (mm)	Base height (mm)	Fin Pitch (mm)	Temperature (°C)
8	2	10	2	4	51.4404
13	2	10	2	4	48.3661
18	2	10	2	4	45.8225
8	1	12	2	4	50.8498
8	2	10	2	4	51.4404
8	3	8	2	4	51.5125
13	1	12	2	4	47.4461
13	2	10	2	4	48.3661
13	3	8	2	4	48.5665
18	1	12	2	4	45.0091
18	2	10	2	4	45.8225
18	3	8	2	4	46.2257
8	1	12	2	4	50.8498
8	1	12	3	4	50.4433
8	1	12	4	4	49.8898
8	2	10	2	4	51.4404
8	2	10	3	4	51.2413
8	2	10	4	4	50.5549
8	3	8	2	4	51.5125
8	3	8	3	4	51.2595
8	3	8	4	4	50.7898
8	1	14	2	3	50.4167
8	1	12	2	4	50.8498
8	1	10	2	5	51.1479
8	1	14	3	3	50.1131
8	1	12	3	4	50.4443
8	1	10	3	5	50.9082
8	1	14	4	3	49.7690
8	1	12	4	4	49.8898
8	1	10	4	5	50.0788

CHAPTER II

The results provided valuable information about heat sink optimization. Those investigated parameters enhance the thermal performance by increment but they have different effects on heat sink efficiency and natural convection development. For this reason, the balance between the enhancement of total thermal performance and efficiency of the cooling component should be studied based on the multi-aspect requirements of the system.

Sapia et al. [13] investigated the effects of vertical rotation of 90° for a horizontal heat sink. Figure 10 and Figure Figure 11 present the velocity profiles for the heat sink before and after 90° of vertical rotation. It is observed that the steady state is reached faster in the vertical orientation case. The natural convection flows are also better organized, and the stagnation areas with low air recirculation speed are reduced. The hot spot temperature of the system was reduced to 51.2 °C from 60.8 °C as the result of a vertical rotation of 90°.

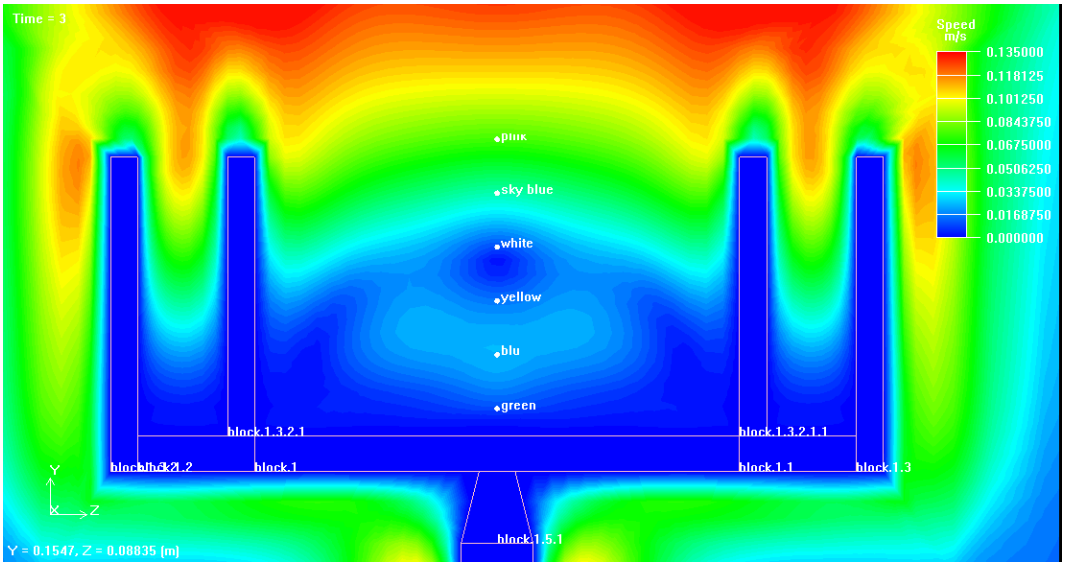

Figure 10: Speed map at t=3s for horizontal orientation [13]

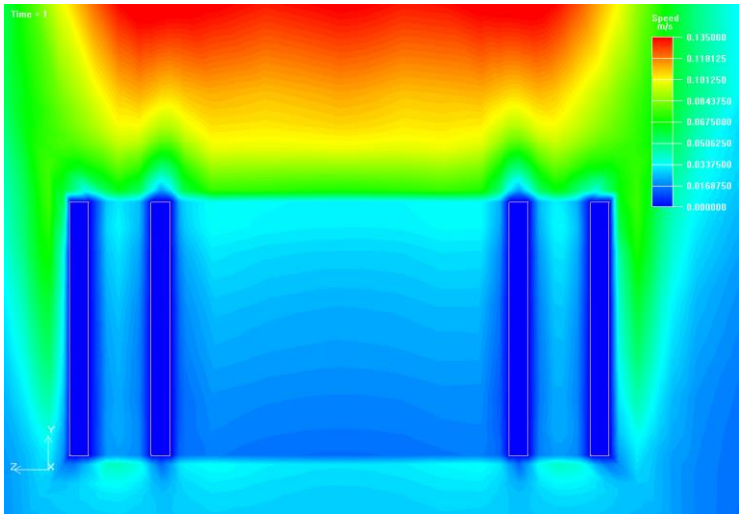

Figure 11: Air velocity map at t=1s for vertical orientation [13]

Dogruoz and Arik [14] investigated the effects of the thermal conductivity and structural parameters of a heat sink on the thermal performance. Computational results of TPG (k=1500 W/m-K) and PPS (k=20 W/m-K) based heat sinks with 60 °C base temperatures are represented in Figure 12 and Figure 13. Figure 12 clearly shows that TPG heat sink efficiently conducts heat within heat sink and dissipates it to surrounding working fluid.

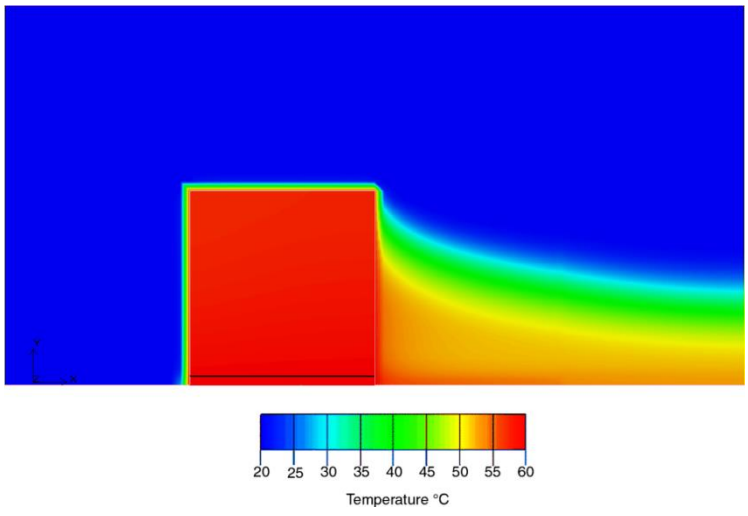

Figure 12: Temperature contours at the mid-plane of TPG heat sink [14]

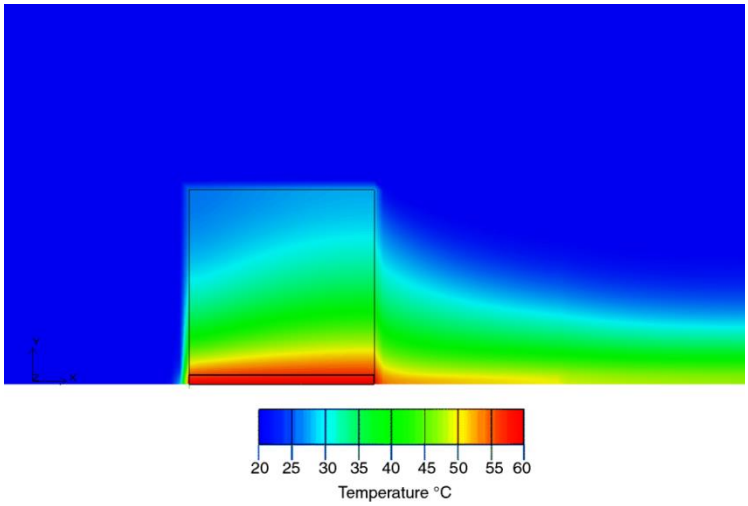

Figure 13: Temperature contours at the mid-plane of PPS heat sink [14]

The effects of fin spacing and thickness based on the FOM (W/kg-K) is represented in Figure 14 for 100 mm fin height, 100 mm fin length, 5 mm base thickness, 60 °C base temperature and 120 W/m-K thermal conductivity for a carbon-foam heat sink. Results show that thin and sparse fin arrangements should be preferred for obtaining high FOM values.

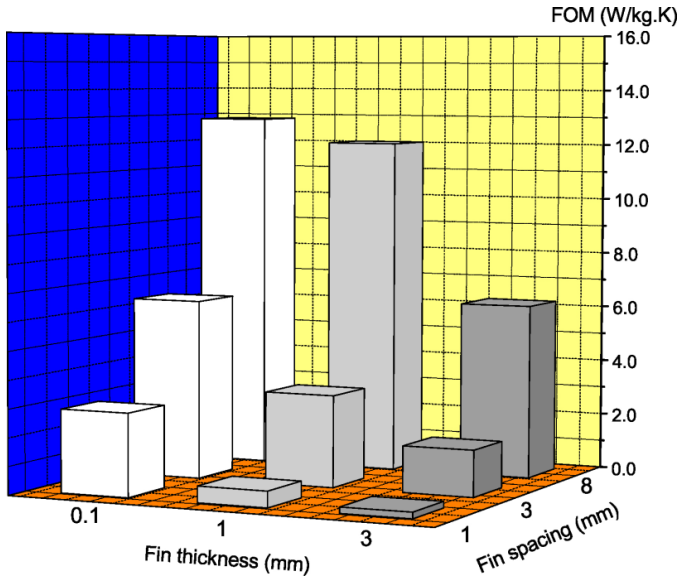

Figure 14: Fin thickness and spacing versus FOM [14]

CHAPTER II

Referred studies are focused on the limitations of passive heat sinks on cooling capacity. A well-designed heat sink should provide effective heat conduction within heat sink, and well-organized and strong natural convection flows.

A research on the development and optimization of a passive cooling approach should be structured due to the operational conditions and requirements of the system. The effect of cooling enhancement on the efficiency and mass should be also studied. Since designing a cooling approach or component is an object far beyond the effort of enhancing only the performance metrics.

2.2 Chimney Effect on Natural Convection Cooling

Chimney effect is a physical phenomenon, which is also used for cooling of electronics besides many other areas. Cooling mechanism based on chimney effect is a natural convection cooling, and feed by itself without receiving any external energy. Natural convection occurs by buoyancy force and results from density and pressure difference due to the temperature changes of a fluid. Chimney effect enhances the natural convection due to the elevated density and pressure difference between heated air in the chimney and ambient air outside the chimney. Major obstacle for application of a chimney inside an electronic device is the space requirement and modification challenge to existing approach structures.

Vermeersch et al. [15] studied the chimney effect on natural convection cooling experimentally. It was emphasized that it is possible to decrease the thermal resistance by 10% even by a small chimney, which has a non-negligible influence on the reliability and the life span in the case of a nominal junction temperature rise of 100 °C. A transistor was used as the heat source and put at the bottom of the chimney as shown in the schematic view of the experimental setup in Figure 15. x value defines

the position of the transistor, which was varying between -20 mm and 40 mm during the experiment for various chimney heights. Best result for a 10 cm chimney height was obtained, when the transistor was just below the chimney inlet (x = 20 mm). For a 30 cm-chimney, x = 0 mm turn out to be the best case, and the case where the transistor was just inside the chimney inlet (x = -20 mm) showed the highest enhancement compared to the case for H = 10cm. This study showed that heat source by the chimney inlet gives the best thermal performance for a sufficient chimney height, and chimney height is a significant parameter that enhances the thermal performance.

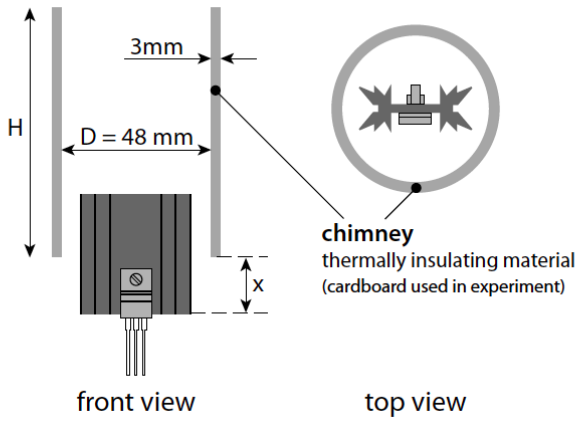

Figure 15: Schematic view of chimney effect experiment [15]

Ishizuka et al. [16] investigated the effect of inclination of the notebook box casing. The experiments are performed for various power inputs and chassis types. A crucial benefit of casing inclination is observed at angles lower than 40° as seen in Figure 16 and Figure 17. This study shows that the inclination angle has a substantial effect on non-vertical chimneys. Ishizuka et al. has also investigated the thermal performance enhancement of higher air outlet position, larger air outlet size and higher distance between heat source and air outlet [17].

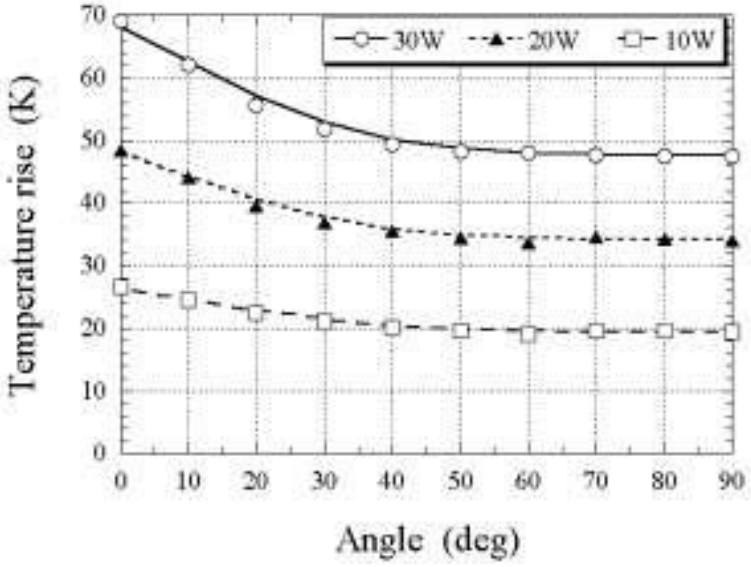

Figure 16: Impact of inclination angle on temperature rise [16]

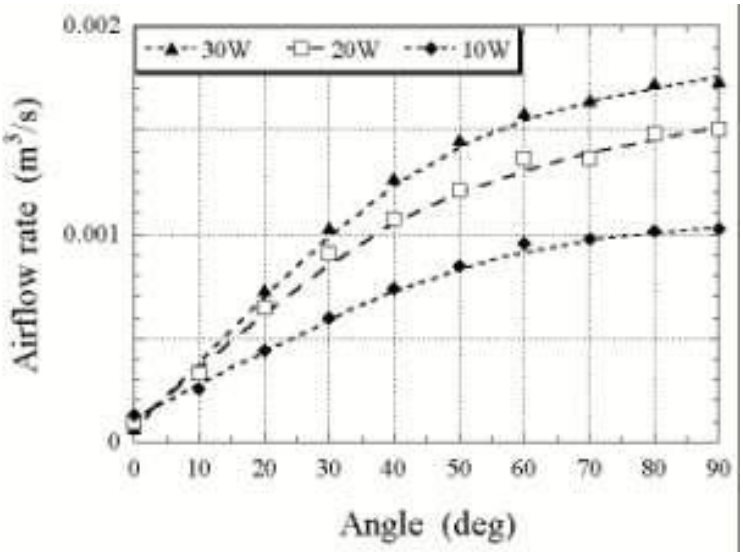

Figure 17: Impact of inclination angle on temperature rise [16]

All studies show that interaction between heat source and chimney structure should be well studied by the optimization of a cooling system based on chimney effect. For the inclined chimney structures, critical angle is a crucial optimization parameter.

CHAPTER II

2.3 Computational Methods in Heat Transfer and Optics

2.3.1 Computational Fluid Dynamics (CFD) Analysis

CFD (computational fluid dynamics) is a practical tool in modern engineering, and it is used for fluid dynamics and heat transfer studies extensively since the beginning of the last decade due to the advancement of computer technologies. CFD presents fast, accurate and cost-effective solutions for complicated problems, which complement the lack of experimental and analytical approaches. Main elements of a CFD analysis are pre-processor consisting of creation of geometry, mesh generation and selection of physics and fluid properties; solver consisting of initialization and solution control, and monitoring convergence; and post-processor consisting of reporting and plotting the results. The discretization of most of the modern CFD software is based on the finite-volume methods (FVM), which are suitable for the conservation equations of compressible flows. Most of the CFD softwares use Reynolds-averaged Navier-Sotkes equations, which models the turbulences in order to solve the problem in an acceptable time. [18, 19, 20]

There may be a number of minor and major error sources in CFD analysis that can manipulate the results. False idealizations, bad or too coarse elements, wrong material data, boundary conditions and solvers are some of those error sources. For this reason, it should not be directly assumed that the results are correct by a CFD analysis. This makes the experience of the engineer crucial to determine and avoid the errors. It is also a task of the engineer to validate the computational results with the experimental results. [18, 21]

In this study, a commercial CFD software, ANSYS Icepak 14.5.2 is used for computational thermal analysis and optimization of developed prototypes. Steps of

each referred main CFD elements are followed, and CFD results are compared and validated with experimental results.

2.3.2 Optical Modeling

Commercial optical modeling softwares are widely preferred today by optical engineers for designing and optimizing the illumination systems. Modeling is a very useful tool, which simplifies and accelerates the design process. High speed calculations give researchers the opportunity to analyze more performance metrics. [22]

Ray tracing methods are used in the optical modeling, which defines a light ray as a line normal to the direction of wave propagation. This enables the simulation of transmission, reflection and refraction of rays through an optical system based on the laws of geometrical optics. Sequential ray tracing techniques are used typically for image-forming systems, when the exact order is known, in which ray strike each surface in the system. Sequential systems are concerned with imaging, and they can compute the ray propagation in a straightforward manner. It is a major task of optical engineering to develop an imaging system that eliminates aberrations, which occur due to any deviations by a point-to-point mapping. Only several hundred rays can be sufficient to analyze the optical characteristic of a sequential imaging optical system completely in contrast to non-sequential illumination systems [22].

Non-sequential ray tracing techniques are used for non-imaging systems like fiber optics, solar concentrators and illumination systems. Since there is no imaging constraint, millions of rays can be required for the analysis. For this reason, non-sequential illumination systems were first started to be widely used by the advent of computerized ray tracing. Many rays determined through Monte Carlo simulation need

to be started randomly from an extended source and traced through system. This analysis enables the placement of a detector at the area of interest and the determination of luminous intensity, luminance and illuminance. The majority of statistical errors occur by the simulation of incoherent extended sources. Statistical accuracy can be ensured by using an adequate number of source rays. [22]

LightTools is an optical engineering software based on non-sequential Monte Carlo ray tracing methods. It supports virtual prototyping, simulation, optimization, and photorealistic rendering of illumination applications [23]. LightTools is used by optical analysis and optimization of the designed prototype for the developed approach in this study.

CHAPTER III

ANALYSIS OF EXISTING LIGHTING APPROACHES

3.1 Methods

In this chapter, various passive cooling approaches and designs are studied, in order to bring the current status of the technology into the table. For this purpose, thermal, optical and electrical setups were designed and developed. Several commercial A-line LED bulbs from world`s leading lighting vendors were purchased and tested in these setups. Seven commercial bulbs (Figure 18) were selected from off-the-shelf systems, and there is no specific reason to choose for a particular brand. To avoid advertisement, no brand name was mentioned in this study. Tested bulbs with various passive thermal solutions are entitled with the names starting from bulb-A to bulb-G.

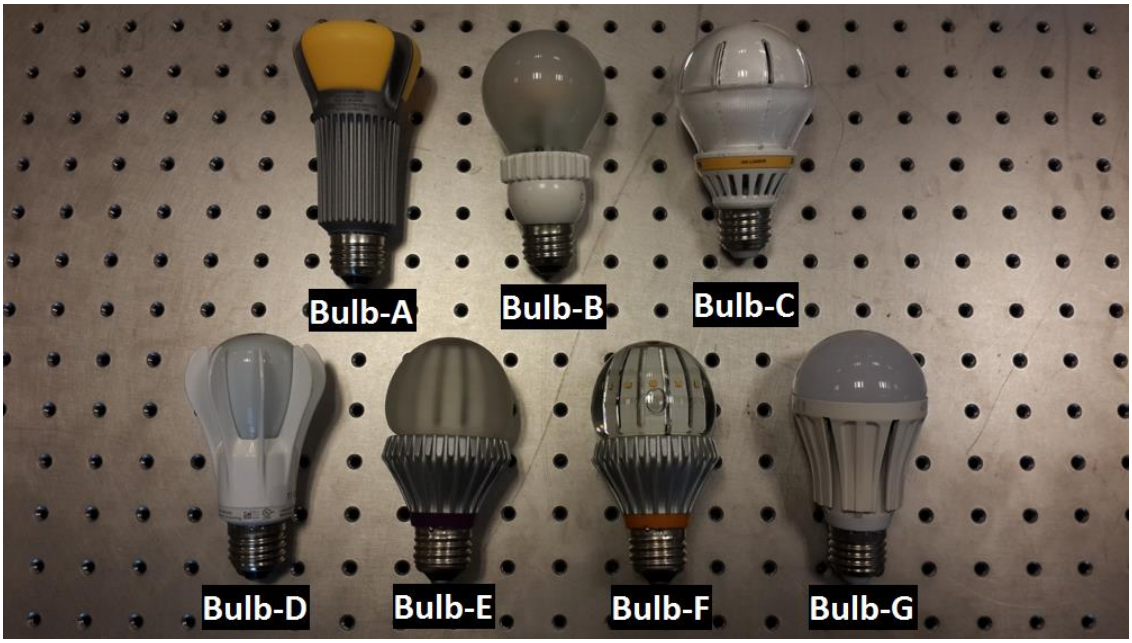

Figure 18: Tested commercial bulbs

CHAPTER III

Chosen bulbs have different input powers, luminous fluxes, weights and sizes due to their designs. They were carefully chosen to compare the opto-thermal performances of different cooling approaches from simple heat sink to external finned complex heat sink and liquid cooling approach. The results display the total system performance of the tested bulbs, but they still enable the interpretation of cooling components. Some of the lamps have different electrical power inputs and light outputs with the same cooling component (Bulb-E and Bulb-F) to indicate their performances under different operational conditions. Information about the cooling approaches and heat sink designs of the bulbs and input powers given by manufacturers are shown in Table 6.

Table 6: Input powers and cooling approaches of test vehicles

Test vehicle	Input power (W)	Cooling approach and Heat sink design
Bulb-A	17	Passive cooling with external fins
Bulb-B	9.5	Passive cooling with small heat sink
Bulb-C	13.5	Chimney effect with internal and external fins
Bulb-D	9	Passive cooling with large external fins
Bulb-E	8	Passive liquid cooling with external fins
Bulb-F	12	Passive liquid cooling with external fins
Bulb-G	10	Passive cooling with external fins

3.2 Experimental Study

An experimental setup was designed and developed to test the thermal performances of various A-line LED bulbs. Bulbs were tested in the air-tight setup created for the experimental study presented in Figure 19. The enclosure was designed with a plexiglas material, and it had a size of 120 x 80 x 90 cm to avoid any external air flows. A standard bulb base was used to screw Edison base lamps. No insulated ceiling structure was used here to simplify the testing procedure, but the thermal test setup still provides adequately accurate results.

Figure 19: Thermal test setup

Test setup was so prepared that A-line bulbs were placed to mimic a real life application. Ambient air in the enclosure was not controlled but constantly monitored during the experiments. It was always in the range of 25±3 °C, which meets the requirements of Energy Star Test Methods [24].

A typical thermal experiment took place over two hours, and steady state temperature measurements have been performed. Steady state decision for temperature was less than ±0.05 K variation in 5 minutes of data collection. Each experiment has been performed at least two times for repeatability and reproducibility, as well as reducing the uncertainty in the readings. An infrared (IR) camera, T-type thermocouples and a data acquisition system were used in the experiments for temperature measurements. For IR thermal measurements, surface emissivities are calibrated with three distinctly located thermocouple readings. A high performance FLIR SC5000 thermal imaging camera provided a high spatial resolution allowing images and also the point measurements with high sensitivity and accuracy [25]. An Agilent data acquisition system was used with T-type thermocouples. Data acquisition and thermocouple system has a special error of 0.5 °C or 0.4 % and a standard error of 1.0 °C or 0.75 % (whichever is greater) [26]. Two thermocouples were placed on lamp glass dome, heat

sink base and heat sink area near to the Edison base to verify the temperature measurements by comparing with each other to ensure the confidence in the emissivity correlation. They were attached to the surfaces with a heat resistant RTV (Room temperature vulcanization) silicone to obtain a reliable contact. Intimate contact of thermocouples with the surfaces was assured by applying controlled pressure. Total system accuracy was adequate enough that no significant deviation for emissivity calibration occurred for the thermal imaging. The error of IR Camera (FLIR SC 5000) is ±1°C [27]. IR images of the tested lamps are shown in Figure 20. Thermal resistances of tested bulbs are shown in Table 7.

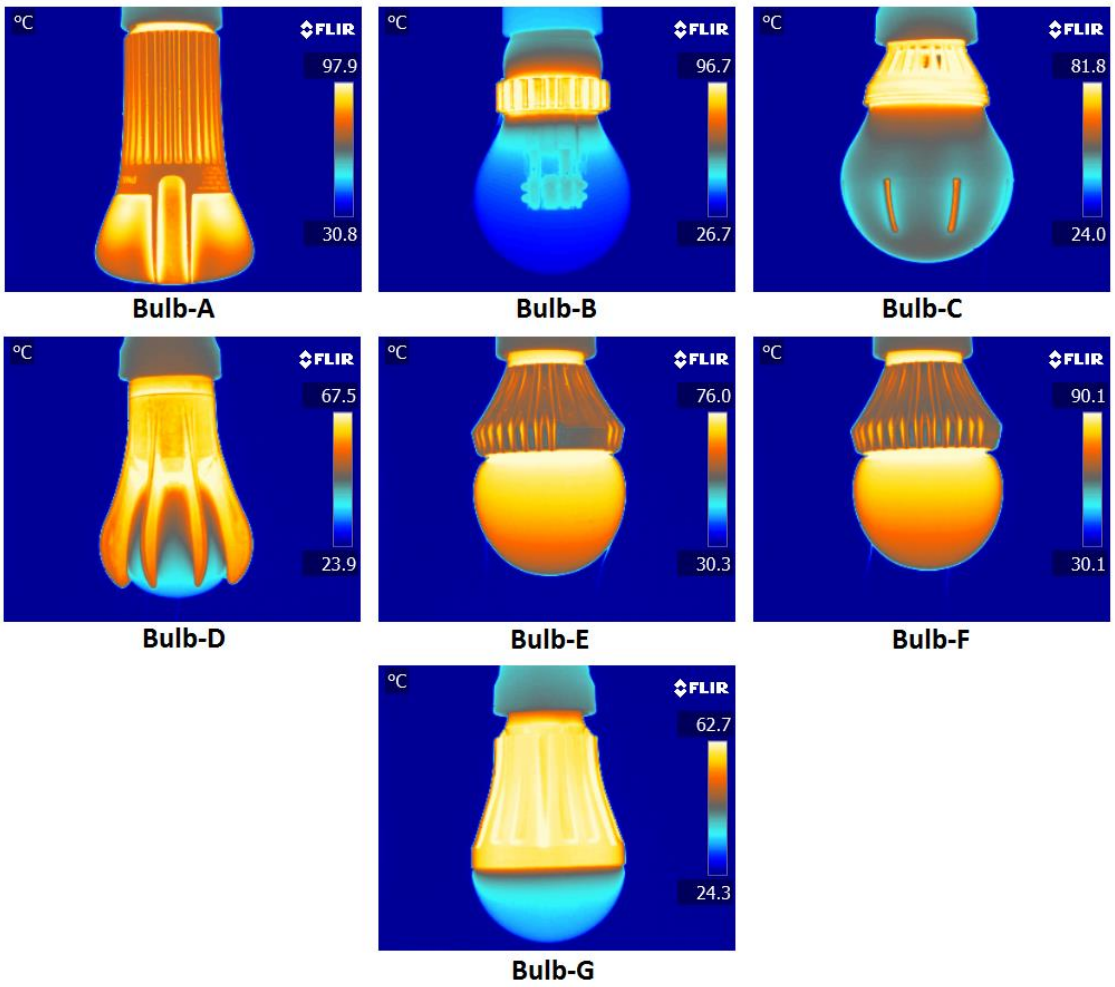

Figure 20: IR images of the tested bulbs

CHAPTER III

Table 7: Thermal resistances of tested bulbs

Test vehicle	Thermal resistance (°C/W)
Bulb-A	5.6
Bulb-B	9.9
Bulb-C	6.1
Bulb-D	6.4
Bulb-E	7.8
Bulb-F	7.2
Bulb-G	5.7

Optical measurements were done in a scientific integrating sphere (SphereOptics) with a diameter of 2 m. The integrating sphere consisting of both photometer and radiometer with a special coating combines 98% reflectance with nearly perfect Lambertian diffusion [28]. Figure 21 presents the preparation stage of the optical measurements in the sphere for luminous flux, color rendering index (CRI), correlated color temperature (CCT). Optical results were obtained, when the heat sinks reached to the steady state temperatures as measured earlier with IR camera and data acquisition system. Both temperature and lumen output reached the steady state values. Integrating sphere was calibrated to the reference bulb before each measurement. Optical results of test samples are shown in Table 8.

Table 8: Optical results of tested samples

Test vehicle	Luminous flux (lm)	CCT (K)	CRI
Bulb-A	1244.0	2633	80.9
Bulb-B	858.6	2723	80.8
Bulb-C	913.3	2986	81.0
Bulb-D	551.5	6535	71.9
Bulb-E	545.0	2642	85.9
Bulb-F	855.0	2772	79.9
Bulb-G	793.0	6483	85.0

CHAPTER III

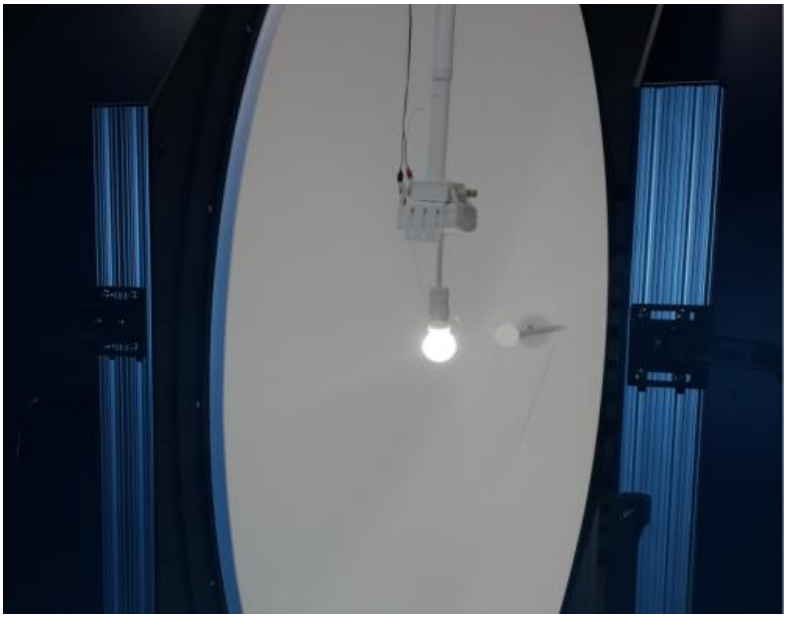

Figure 21: Optical test setup

Surface area calculations were taken from CAD models for each lamp. Weight was also experimentally measured for combined performance analysis based on the new FOMs. Uncertainty in the weight measurements was less than 1%. Real consumed powers of lamps are measured with an Agilent digital storage oscilloscope under steady state conditions in thermal tests. Results for the surface area, weight and input power are shown in Table 9.

Table 9: Weight and surface area of tested lamps

Test vehicle	Weight (g)	Surface area (cm^2)	Input power (W)
Bulb A	223	173	17.0
Bulb B	115	33	9.8
Bulb C	227	265	12.3
Bulb D	123	104	8.7
Bulb E	276	113	7.4
Bulb F	273	113	10.7
Bulb G	112	149	9.4

CHAPTER IV

CONCEPTUAL, NUMERICAL AND EXPERIMENTAL STUDIES FOR NEW APPROACH

4.1. Development of Baseline Concept

A 100 W incandescent equivalent A-line LED bulb with 1700 lm luminous flux is one the important requirements of the lighting market. For such an LED bulb a cooling capacity of at least 14 W should be provided, when the various efficiencies of LEDs and electronic driver circuits are considered. Thermal resistance is a figure of merits, which give reflects the cooling capacity of a system. For a junction temperature limit of 110 °C and an ambient temperature of 55 °C (Energy Star requirement in elevated temperature life testing [24]), thermal resistance should be a maximum of 3.9 °C/W. An ambient with a temperature of 55°C is actually an extreme case and may be seen rarely in operational conditions for this type of LED bulbs. A temperature of 110 °C is also determined as the highest junction temperature advised by a number of manufacturers, although many LEDs can function at higher temperatures. Hence a 3.9 °C/W of thermal resistance ensures both a safe operation for the extreme conditions, and high performance and reliability for the usual conditions.

As studies showed, even only the heat sink thermal resistances of passive thermal management approaches of existing A-line bulbs are much higher than 3.9 °C/W. A new approach and concept of design based on chimney effect can have a sufficient thermal performance in contrast to existing ones, which reach their limits. Cooling approaches based on chimney effect are already used in some electronic systems and showed high thermal performances. Nevertheless, use of a chimney for A-line LED bulbs was limited due to current structure approaches and

form factors. A chimney based thermal management needs to be carefully structured with several consideration points.

Prior studies showed that heat source should be located carefully in order to utilize the chimney effect. Since there are LEDs and electronic driver circuit as heat sources in an LED lamp, it is a more complicated task than by usual chimney cooling approaches. Chimney structure, positions of heat sources relative to chimney and each other are the parameters that identify the thermal performance. Thermal management of electronic driver circuit should also have the primary priority. It is a matter of very high heat fluxes over electronic components, even when the efficiency is high as 90%, since input power should be approximately 18-20 W. Direction of natural convection flows should not sustain any important angle changes by air inlet, flow path inside the system or air outlet. Thermal resistance goal of a 3.9 °C/W imposes the implantation of a finned structure inside the chimney, since the surface area inside the chimney is very limited for an adequate cooling capacity. The requirement of omni-directional and homogeneous luminous intensity distribution is one of the main obstacles for the application of a chimney based thermal management. The optical design needs be embedded in the thermal design, which brings the requirement of an opto-thermal system design. Since optical and thermal designs cannot be separated from each other, they should complete each other and meet the requirements of each other. The design of an LED array determines both the luminous intensity distribution and the positions of heat sources. The diffuser design and the chimney structure are in a tight interaction with each other, which structures the natural convection flow path and determines the light diffusion and the reflection parameters. PCB and heat sink base have thermal and optical effects on system as well. Electrical connection from Edison base to LEDs over an electronic driver circuit and mechanical durability of the system are other important consideration points of design.

CHAPTER IV

The LED array of a chimney-based concept can be designed horizontally or vertically, as seen by some of the tested bulbs. A simple horizontal array with light guide can substantially provide an omni-directional and homogeneous luminous intensity distribution. However, the form of light guide diminishes the chimney structure and limits the size of air inlet. Vertical LED array has the lack of the forward intensity distribution. For these reasons, a new approach is aimed to be developed that will bring an opto-thermal system solution. An LED array, which is angularly positioned to the center line, can give a very wide range of options for homogeneous luminous intensity distributions. This even suspends the requirement of the diffusion property of the component, which is usually called diffuser.

A high transparent material such as glass can also be used for the protection of the light engine, and this can minimize the light absorption in this component. Heat sink base, where the light engine is placed on, constitutes also the chimney. According to this new approach light engine is placed directly on the chimney, which shortens the thermal path and minimizes the thermal resistance due to conduction heat transfer. This also gives an opportunity to position the heat sources on the chimney as desired, which is crucial as many studies showed. An important problem of the most of the existing approaches is the free space inside the diffuser. This space mostly wastes an important part of reserved volume with no main thermal or optical purposes. New approach minimizes this unused free space and utilizes this for creating a chimney and increasing the heat removal capacity. Well-designed natural convection flows guided by buoyancy force are expected to follow the reserved flow path due to a small inclination angle of chimney. Electronic driver circuit is also positioned in the center of the heat sink, which is directly on the natural convection flow path.

Thermal resistance due to conduction heat transfer is also very limited for electronic driver circuit located in the middle section of the heat sink. This part also guides the natural convection flows and utilizes them for the cooling of electronic driver circuit. Fins between the middle section of the heat sink and the heat sink base are directly on the path of natural convection flows caused by buoyancy effect and cool both LEDs and electronic driver circuit with an effective utilization of natural convection flows. These are also mechanical connections between heat sink parts. CAD model of the prototype was created according to A19 standards of ANSI based on the mentioned design considerations, which can be seen in Figure 22.

Figure 22: CAD model of designed prototype

The number and the type of LEDs is crucial and also affects the optical design parameters like heat sink base angle. A light engine of high power (HP) XPG-2 LEDs with a 115° viewing angle was intended to be created, since it has

sufficiently homogeneous luminous intensity distribution and also a luminous flux of more than 1700 lm for 500 mA driving current.

The preferred number of LEDs makes it possible to surround the chimney with heat sources in order to create well-designed uniform natural convection flows. A number of trapezoid heat sink bases were brought together to create the chimney. MCPCBs were also created with the same geometry of trapezoid bases. These MCPCBs aim an effective heat spread on the heat sink base. The structure consisting of trapezoid bases creates a chimney near to round profile, which is vertically expanding in flow direction. Fins have a minimum fin spacing of three times of the fin thickness, which is 1 mm. The system structure is represented in cross sectional view in Figure 23.

Figure 23: Cross-sectional view of designed prototype

CHAPTER IV

4.2. Thermal Resistance Network

Analytical models and calculations are used for fast and cheap analysis of heat transfer problems. Assumptions and idealizations of material properties, boundary conditions and geometries are used to make the problem so simple that it can be solved analytically with simple heat transfer equations. Thus, three modes of heat transfer can be expressed as 1D heat transfer problem. Thermal resistance is represented by using Ohmic resistors used in electrical networks due to the analogy between heat diffusion and electrical charge. Resistors can be connected in series or parallel as in electrical networks. Thermal resistance network gives researcher the opportunity to study the thermal scheme consisting of all components based on heat removal mechanisms. A simplified thermal resistance network is created for the fast analysis of the developed prototype (Figure 24).

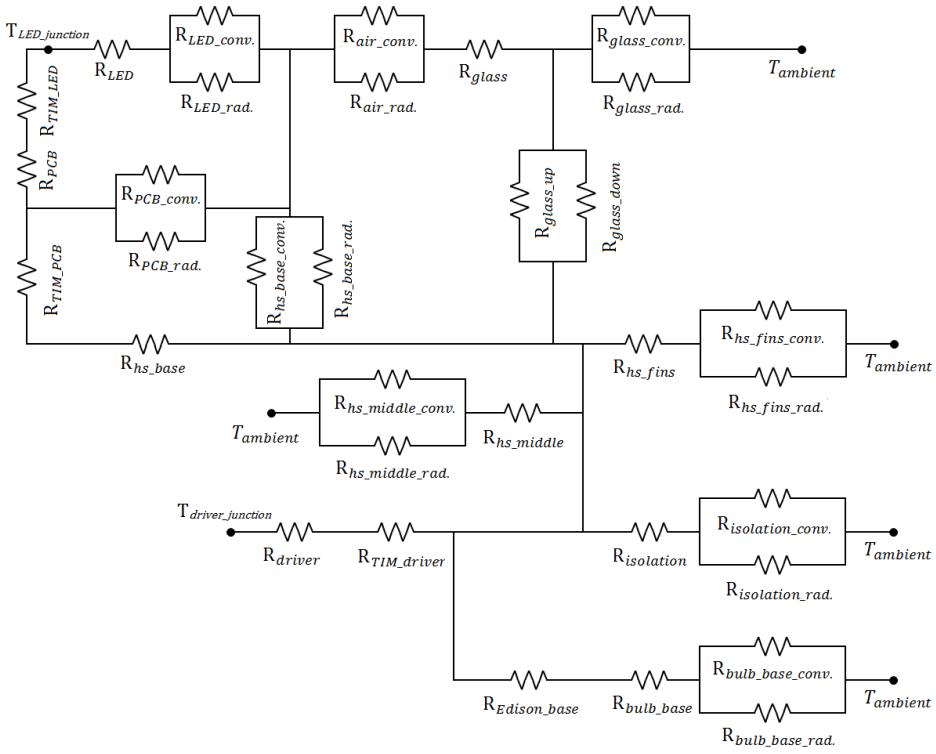

Figure 24: Thermal resistance network of developed LED lamp prototype

CHAPTER IV

All components of the system are assumed to have planar geometries so that the problem can be handled as a 1-dimensional heat transfer problem as represented in Figure 24. For many LED lighting systems, 80-90% of heat is generated in LEDs. Therefore, thermal resistance network between LEDs and ambient air has the highest priority. Heat transfer from driver to heat sink is remarkable as well. Very small heat transfer in base direction has the lowest priority here. LED Junction temperature point is determined between LED and TIM, because it is the closest point to junction of the LED. R_{LED} represents the thermal resistance of 12 parallel-connected LED chips for heat conduction. Heat sink thermal resistance is divided into three parts as base (R_{hs_base}), fins (R_{hs_fins}) and middle section (R_{hs_middle}), so that heat spreading properties of heat sink base and middle section can be respected. Thermal resistance for natural convection ($R_{conv.}$) and thermal radiation ($R_{rad.}$) are in parallel connected for all surfaces exposed to ambient air, since both of them remove heat from surface to ambient at the same time.

Thermal resistance scheme is a good overview for understanding and improving a thermal system, but it is not easy to simplify the developed system to 1D heat transfer problem accurately especially for the developed heat sink due to the complex geometry of the system. From this reason, new approach is computationally analyzed by using a commercial CFD software in this study, and computational results are validated with experimental results.

4.3. Computational Studies

4.3.1. Optical Modeling

Optical design of the system is investigated in this section through LightTools 8.1.0. By the conceptual design, LED array was planned to be angularly positioned to the center line. The number of LEDs is crucial in this study for a homogeneous

luminous intensity distribution, and luminous flux goal was 1700 lm as explained in Chapter 4.1. An LED array consisting of CREE XPG-2 LEDs with 115° viewing angle was studied based on various base angles between 0° and 90° by the computerized analysis. XPG light sources taken from LightTools library were placed on various CAD model, and 10,000,000 rays were used for each analysis.

Results showed that this approach gives a very wide range of luminous intensity distribution opportunities, while some of them can be very applicative for A-line lighting systems. Polar diagrams for the base angles with 5° increment obtained through a receiver 2 m away from the light engine can be seen in Figure 25 respectively.

Since the designed illumination system of new approach has a good luminous intensity distribution, dome of the bulb was a high transparent and non-diffuser material, which reduces the absorption of emitted light. Even when the bulb should be used with a diffuser, light intensity distribution is not expected to show a considerable difference due to the optical design of the system.

A base angle with 350 cd luminous intensity in forward direction was preferred, since forward intensity distribution was aimed. Polar diagram for light engine structure with the preferred base angle can be seen in Figure 26. This light engine was used for the development of prototype.

CHAPTER IV

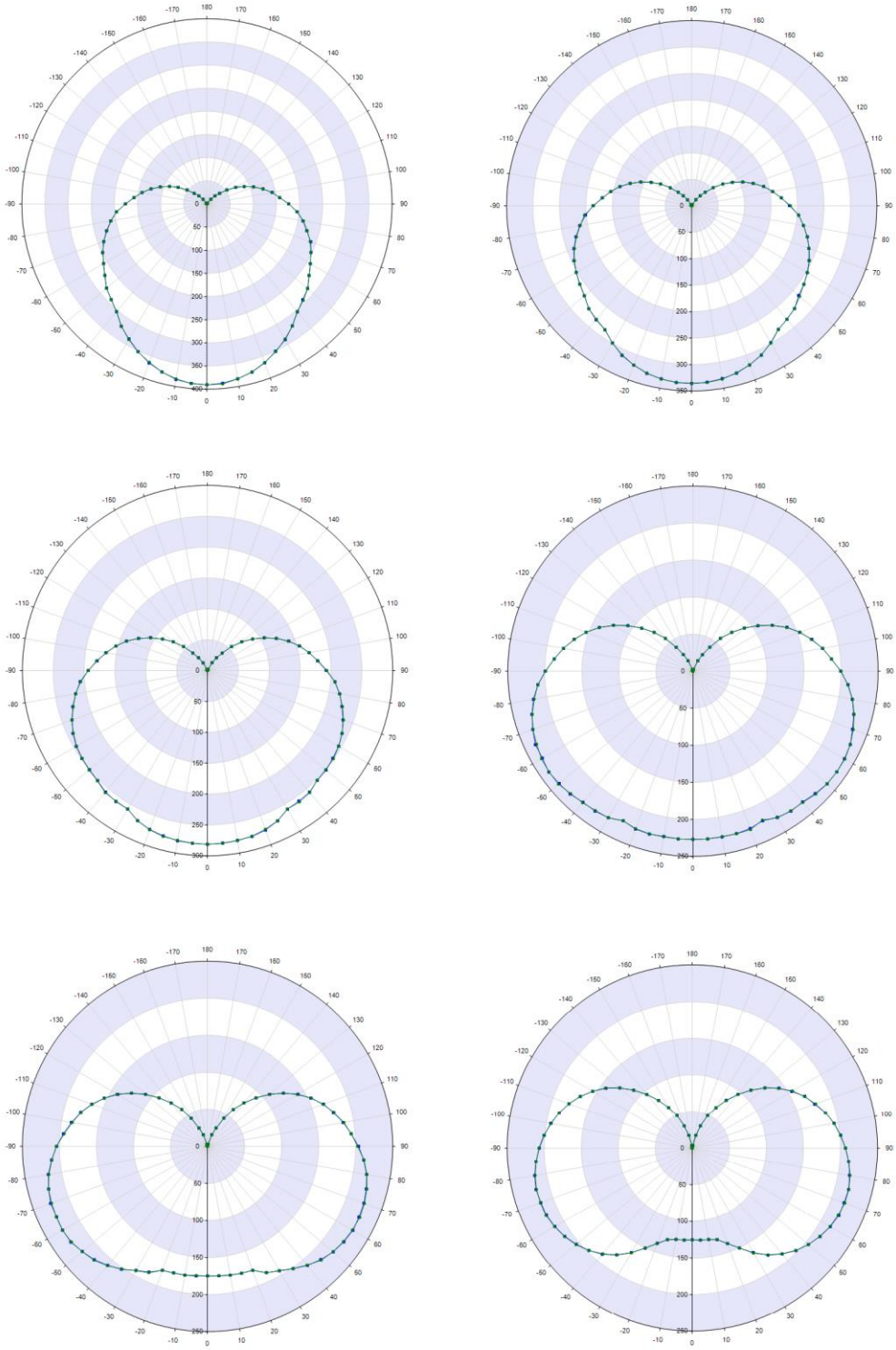

Figure 25: Polar diagrams for various base angles

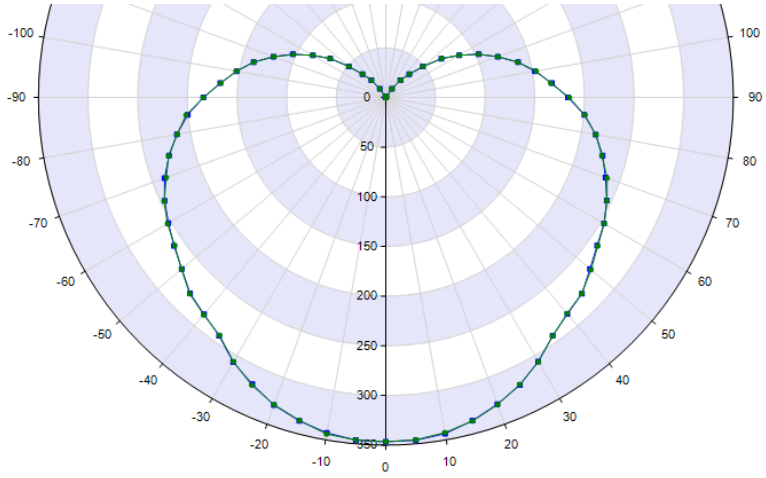

Figure 26: Polar diagram for preferred base angle

4.3.2. CFD Analysis

In this section, two different CFD analyses are performed. First analysis shows the pure thermal performance of the system, while second analysis aims to simulate the experimental conditions to evaluate the system under actual conditions so that it can be compared with the tested commercial lamps. In order to perform the analysis, CAD models were created by a commercial CAD software (Creo). Then, these CAD models were imported to a commercial CFD software (ANSYS Icepak 14.5.2) for the computerized thermal and fluid analysis. Obtained results provide comprehensive thermal maps showing the temperature contours and local temperatures used for the validation with the experimental results.

4.3.2.1. CFD Analysis for LED Simulating Heater Tests

Analysis of the system with heaters involves only the indispensable components of the system for a thermal analysis. These are heat sink, dome and heat sources. Since these components were intended to be manufactured and tested, computational design was also performed with the properties of manufacturing materials. Al-6082-T6 was used for heat sink, which was intended to be

manufactured with a 5-axis CNC (Computer Numerical Control) machine. Polyimide heaters were placed on the heat sink base as heat sources, which simulated LEDs. In this way, heat flow rate was able to be directly controlled only in a single step. Dome was an opaque PMMA material, which was intended to be produced with a 3D printer. In this test method, no light-generating components were used, and there was no optical purpose of dome. Since the dome in heater test simulated only the thermal behavior of actual dome, it was worthy to use a cheap, easy manufacturable and opaque PMMA dome for this study.

Space for the electronic driver circuit was filled with a PMMA material, which was intended to be produced with a 3D printer again. Thus, no extra heat dissipating area was added to the system, which helped to analyze the pure thermal performance of the system. In addition to being easy, fast and accurate, this method is also cheap and do not require an important utility without a standard thermal measurement setup. Only so many heaters with the number of light engines and 3D printing machine are required. This method can be used as a standard test method for system level thermal analysis of SSL lighting systems. CAD model created for the first analysis can be seen in Figure 27.

Figure 27: CAD model for heater test (cross sectional view for dome)

CHAPTER IV

CAD model was converted into an Icepak model with a very fine facet quality for an accurate CFD analysis. Thermal conductivity of heat sink was defined as 160 W/m-K. Thermal conductivity of used aluminum was determined by the experimental thermal conductivity test, which will be showed in Chapter 4.4.1.2. The emissivity of heat sink surface was defined as 0.95. Emissivity was also obtained as a result of an experimental test, which will be showed in Chapter 4.4.1.1. The emissivity of all other undefined surfaces was 0.8 as default.

Thermal conductivity of the PMMA dome and driver space filling component was defined as 0.2 W/m-K. Heaters were defined as high thermal conductive 3D heat sources with a total power of 14 W. Bulb was suspended in the middle of the cabinet with a size of 200mm, 300mm and 200mm in x, y and z directions. Ambient temperature was 26.6 °C, which was provided in the experimental test later. Discrete ordinates radiation model and zero equation – turbulent flow regimes were preferred due to the geometry of the system and occurred Reynolds number. Gravity force was defined in vertical dome direction for simulating the natural convection development under actual conditions. A hex-dominant mesh was used in the analysis. Maximum element size defining maximum element length in x, y, and z coordinate directions was set to 5 mm. Minimum gap specifying minimum distances separating objects was 2 mm. A non-conformal assembly including 5 mm vicinity of system in positive and negative x, y, and z coordinate directions was formed to refine the mesh in the critical region. Maximum element size was 2 mm and minimum gap was set to 0.5 mm for non-conformal region. Multi-level meshes and uniform mesh parameters were enabled to resolve the fine-level-features, and create non-conformal meshes and uniform mesh sizes. Element number of refined mesh was 1.319.507 (Figure 28). Isolines on the mesh visualization occurred due to the solid filling of objects, which was preferred for visibility. Maximum heat sink temperature for various mesh structures

can be seen in Figure 29. All CFD analyses in this study were carried out by using the convergence criteria of $1e^{-10}$ for the flow in x,y,z directions and $1e^{-7}$ for the energy, which was reached after approximately 1500 iterations for the heater test. Results can be seen in Figure 30, Figure 31, Figure 32, Figure 33, Figure 34 and Figure 35.

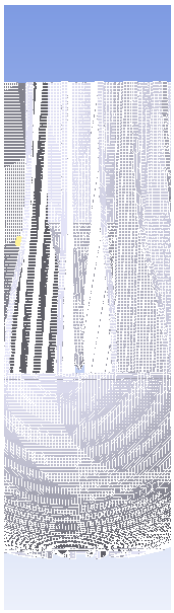

Figure 28: Mesh visualization of Icepak model

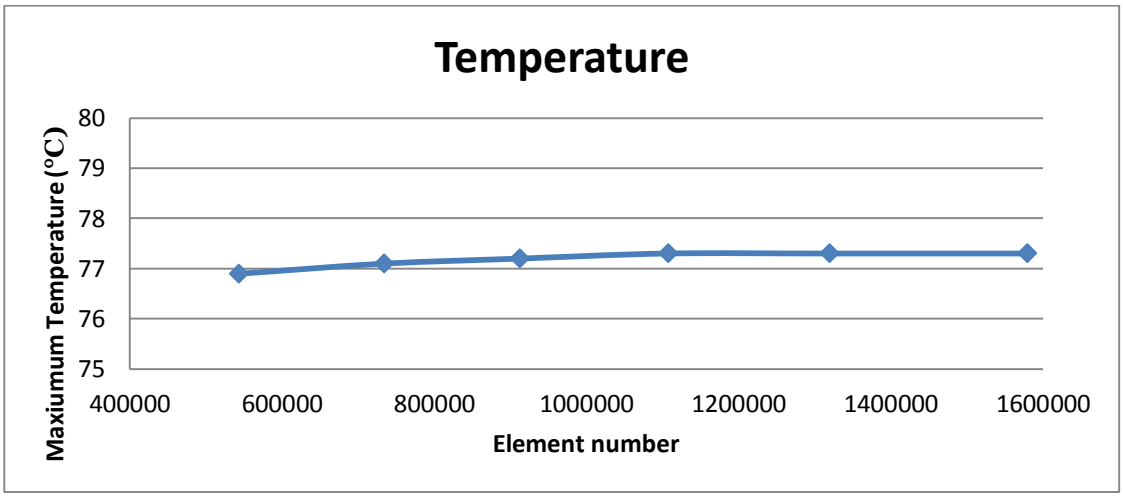

Figure 29: Maximum heat sink temperature for various mesh structures

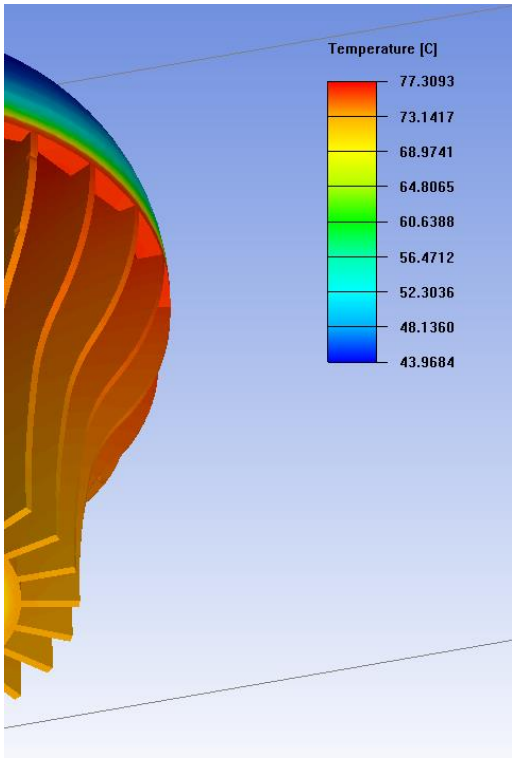

Figure 30: Temperature contours on prototype

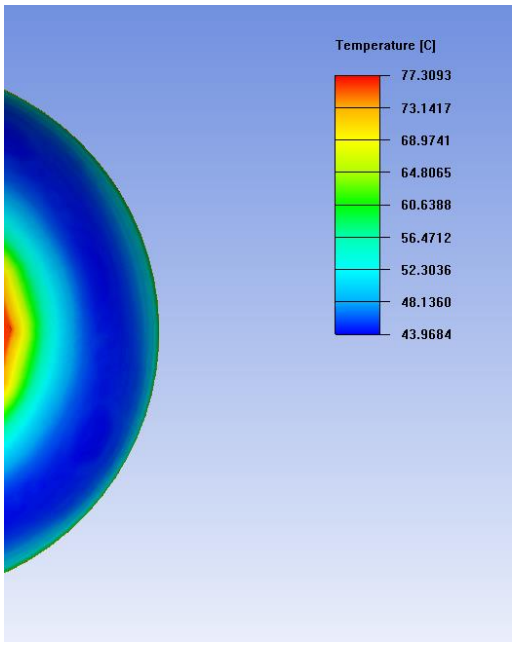

Figure 31: Temperature contours on prototype

CHAPTER IV

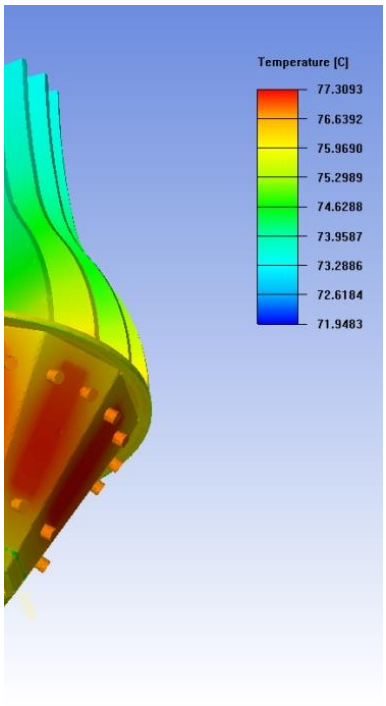

Figure 32: Temperature contours on prototype

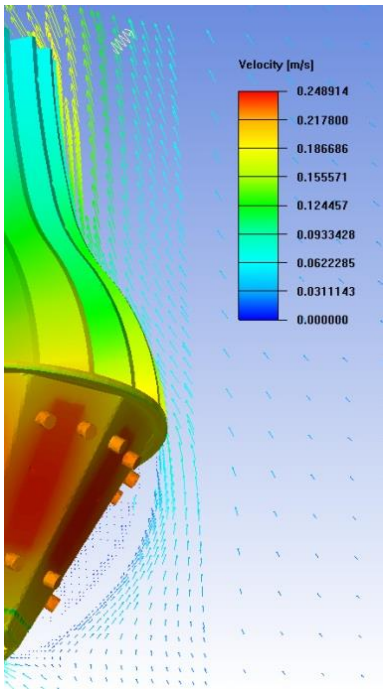

Figure 33: Temperature contours and velocity vectors

Plane cut contours for temperature (Figure 34) shows how working fluid enters the chimney and is heated effectively during passing through the fins. Plane cut vectors for velocity magnitude (Figure 35) shows the match of the system geometry with the natural buoyancy flow direction and proper natural convection development inside heat sink. It is observed that thermal behavior of heat sink is similar to heat sinks with vertical bases thanks to sufficient high base angle.

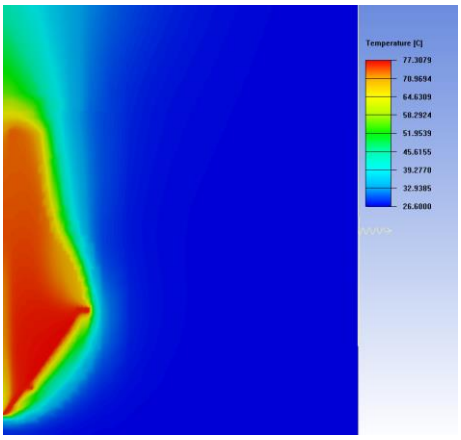

Figure 34: Plane cut contours for temperature (5.5 mm away from center)

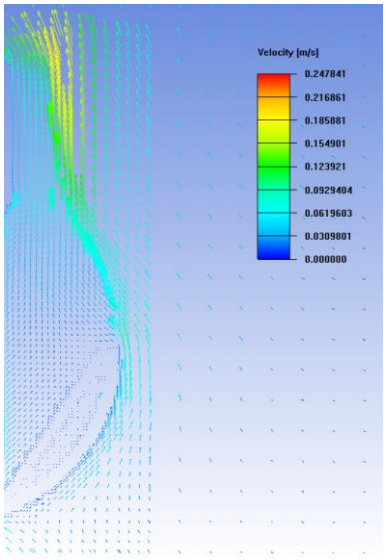

Figure 35: Plane cut vectors for velocity magnitude (5.5 mm away from center)

CFD results show that maximum heat sink temperature was 77.3 °C, which means a 3.6 °C/W thermal resistance for 26.6 °C ambient air. Figure 30 shows the small temperature gradients on heat sink indicating that heat is efficiently transmitted within heat sink. The fact that mean temperature of heat sink is 75.3 °C verifies the efficiency of the heat sink as well. It is also observed that heat is effectively spread on the heat sink base thanks to expanded LED array on 3-dimensional large base area. Due to the plane cut visualization, it is also observed that some ambient air passing through the outside of the dome enters the fin spacing again and cools the fins. Those computational findings explain the high thermal performance of the system. Only noticeable issue according to results was the minimum temperature of heat sink on the top part. 72.0 °C of minimum temperature means a temperature difference of 5.3 °C within heat sink. This difference occurred due to the fact that the analysis was carried out only with heaters. Under actual conditions, there will be a heat generating electronic driver circuit in the middle section, which will utilize the unemployed cooling capacity in this part.

4.3.2.2. CFD Analysis for LED Packaged System

In the second analysis, thermal performance of the system under actual conditions was investigated, after the pure thermal performance of the system has been analyzed by offering a practical and highly-controlled test method. Analysis of the system with LEDs was carried under actual conditions of previous experimental tests. For this purpose, a new CAD model including LEDs, PCBs, isolation, Edison base and standard bulb base was carried out. PMMA isolation was intended to be produced based on the CAD model. E26 base and standard bulb base were created based on the actual ones, which were used by the experimental tests. Edison base was standard aluminum again and bulb base was plastic including copper wire inside in CAD models. Edison base was placed into the bulb base carefully just as

in the actual conditions to obtain the same natural convection development. LEDs were simplified as high thermal conductive 3D heat sources on MCPCBs, since only the surface temperature was in the field of interest. Assembled CAD model for the second analysis can be seen in Figure 36.

Figure 36: CAD model for LED test

An Icepak model was created through the CAD model again. Material and surface properties were not changed for the existing ones in the first analysis. Thermal conductivity of transient PMMA dome, PMMA isolation and bulb base was defined as 0.2W/m-K. TIM material with a thermal conductivity of 0.9 W/m-K and thickness of 0.2 mm was used between heat sink base and PCBs. Thermal conductivity for copper wire inside the bulb base was 400 W/m-K. Thermal conductivity of MCPCB was 150W/m-K by simplifying it to a standard aluminum plate [10]. While ambient temperature was 25 °C this time, other boundary conditions were same as in the heater test. Maximum elements size was 1 mm and minimum object gap was 0.5 mm in non-conformal region in contrast to the first analysis. Number of elements was 1.667.497 for the mesh (Figure 37). Maximum

heat sink temperature for various mesh structures can be seen in Figure 38. Results can be seen in Figure 39, Figure 40, Figure 41, Figure 42, Figure 43, Figure 44 and Figure 45.

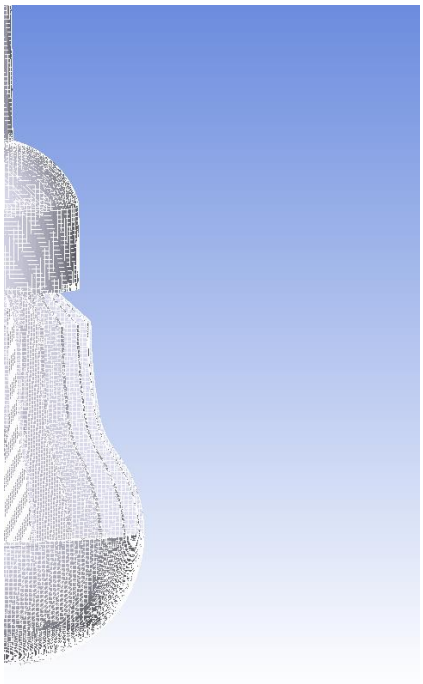

Figure 37: Mesh visualization of Icepak model

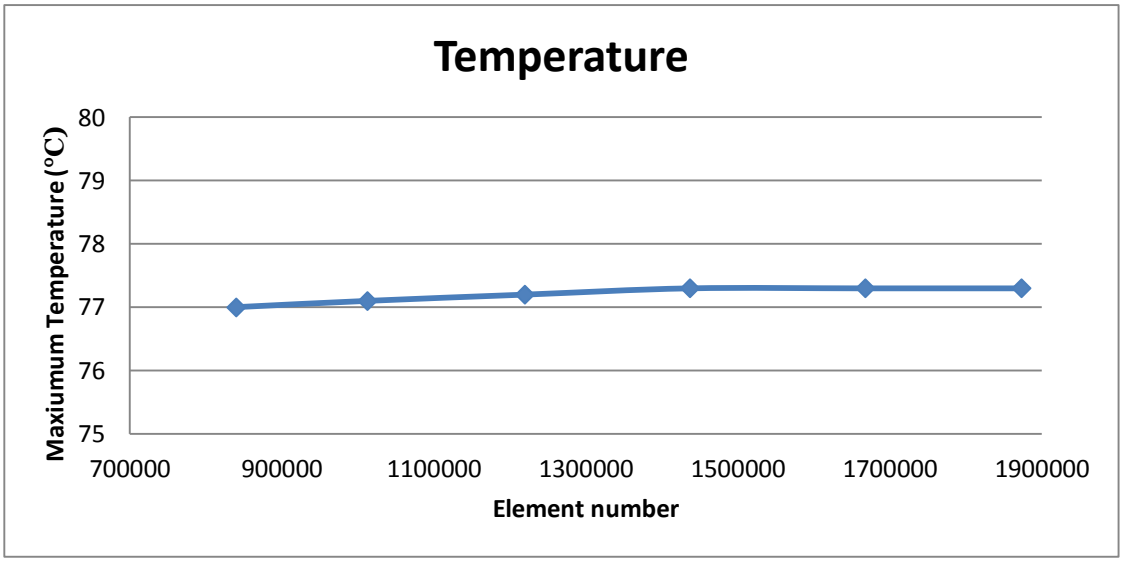

Figure 38: Maximum heat sink temperature for various mesh structures

CHAPTER IV

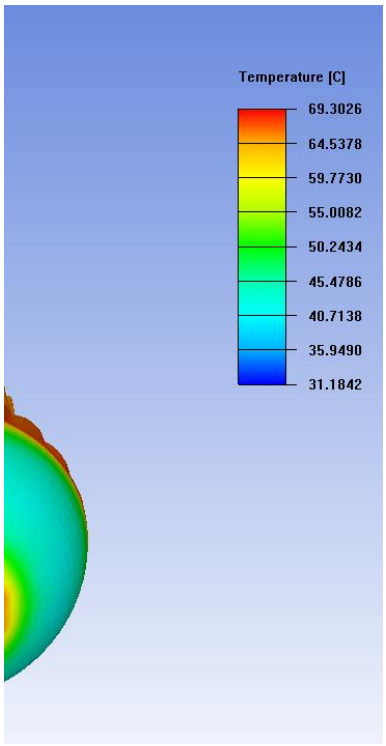

Figure 39: Temperature contours on prototype

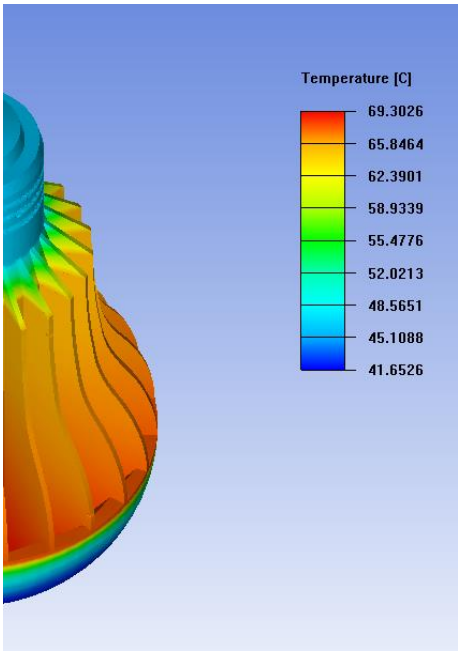

Figure 40: Temperature contours on prototype

CHAPTER IV

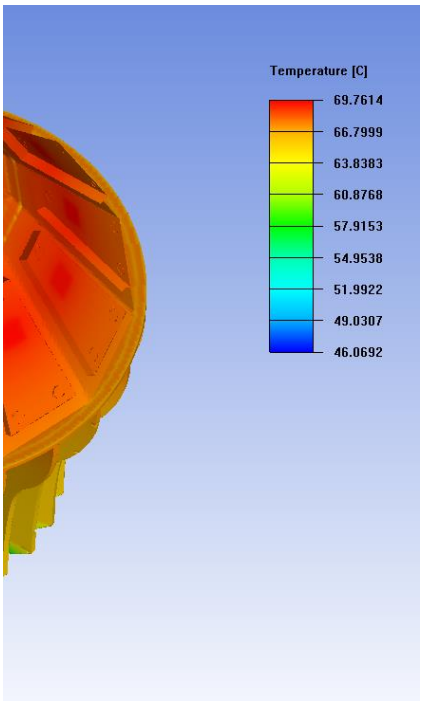

Figure 41: Temperature contours on prototype

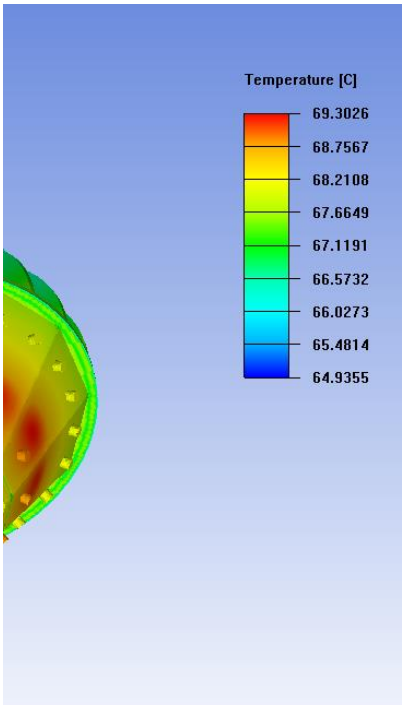

Figure 42: Temperature contours on prototype

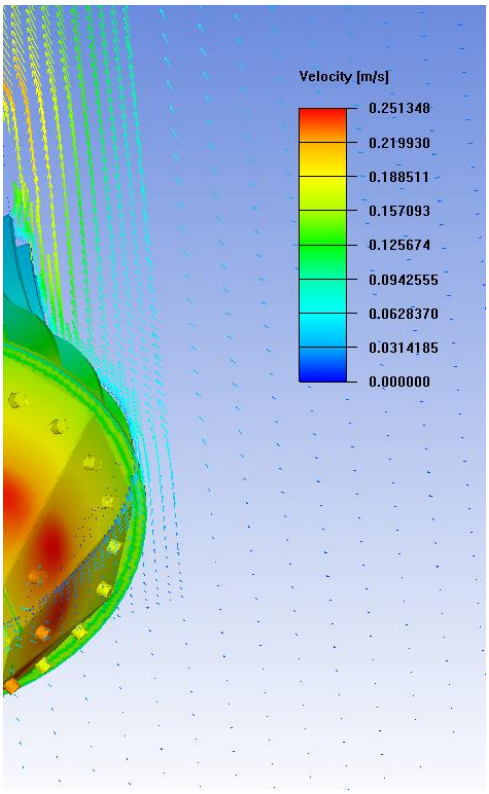

Figure 43: Temperature contours and velocity vectors

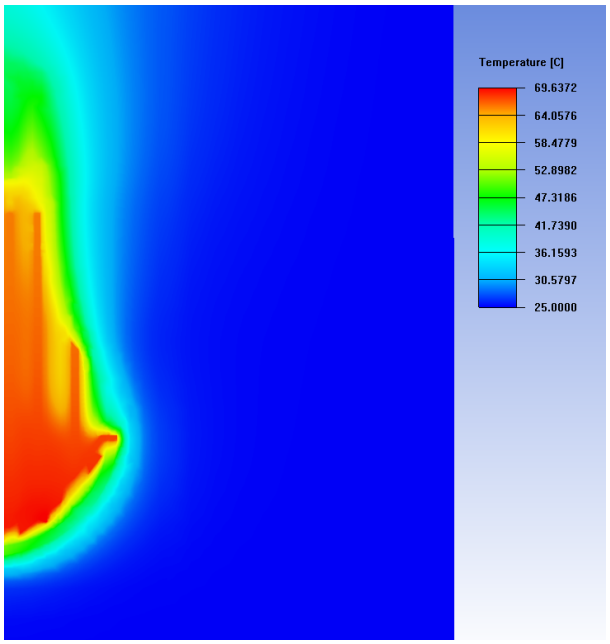

Figure 44: Plane cut contours for temperature (9.5 mm away from center)

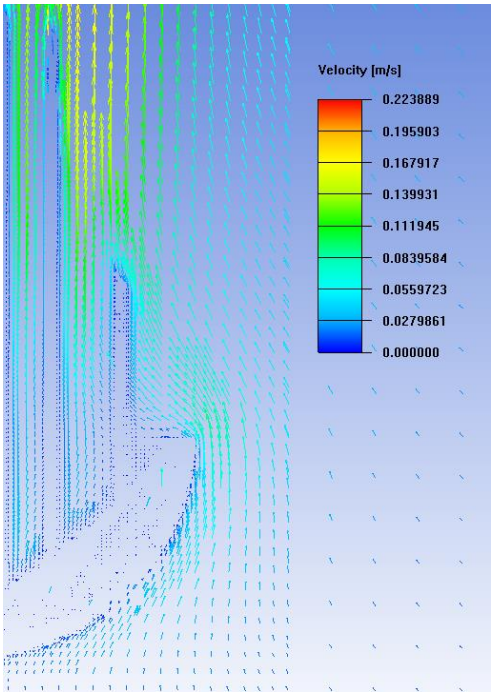

Figure 45: Plane cut vectors for velocity magnitude (9.5 mm away from center)

In addition to obtained results in heater analysis, Figure 41 shows that MCPCBs spread heat to the heat sink base effectively. Figure 42 shows that heat zones of LEDs are not in intersection. Plane cut for temperature (Figure 44) and velocity magnitude (Figure 45) show the proper natural convection development inside the heat sink.

Thermal resistance in the second analysis was 3.9 °C/W with a maximum heat sink temperature of 69.3 °C, and a mean temperature of 67.2 °C. This is 8.3% higher than the thermal resistance obtained in the pure thermal performance test. It can be explained by the bulb base as an obstacle to buoyancy flow. A thermal resistance of 3.9 °C/W still represents a very high cooling capacity even compared to bulb-A of global vendor with the lowest thermal resistance of 5.6 °C/W among the tested bulbs. Another important point is that the system design is performed originally for cooling of both LEDs and electronic driver circuit. Total temperature difference

within heat sink is 4.4 °C. By integration of an electronic driver circuit in the actual case, another heat source will be positioned in the middle of the heat sink. Since cooling capacity here is not totally employed by LEDs, cooling of electronic driver circuit with high heat flux and primary priority will be ensured. This will increase the efficiency, and thermal resistance under actual conditions is expected to be lower than computed results.

4.4. Experimental Studies

This section presents the thermal studies for determining the emissivity of a high heat paint, determining the thermal conductivity of the heat sink material and thermal analysis of the manufactured prototype. This section also consists of experimental studies for optical performance analysis of manufactured prototype. Manufacturing details are given in the sections of related experimental studies, since various components are manufactured for the mock-up heater test and LED tests as intended by the computational study. All thermal tests were carried out in the thermal setup, which was described in Chapter 3.2. All test methods, conditions and errors are same for these tests as in Chapter 3.2, if a new one is not specified.

4.4.1. Thermal Studies

4.4.1.1. Emissivity Study

An infrared (IR) camera is one of the essential devices in a thermal test setup, since it enables the thermal mapping of the system in detail. By using an IR camera, emissivity of the monitored surface for thermal radiation should be known in advance. This brings the necessity of painting the surfaces of the object with a specific paint for IR monitoring. It is also important for bringing the whole surface into the same properties so that the thermal behavior of the object can be monitored properly and correctly. A high heat spray paint with a high emissivity was intended

to be used in thermal tests. For determining the emissivity of the paint, a copper plate was prepared with the dimensions of 0.2 x 85 x 85 cm. High conductivity and small thickness of copper plate was important for the easy determination of emissivity through small temperature gradients on the surface. One side of the copper plate was covered with a flexible heater (Figure 46).

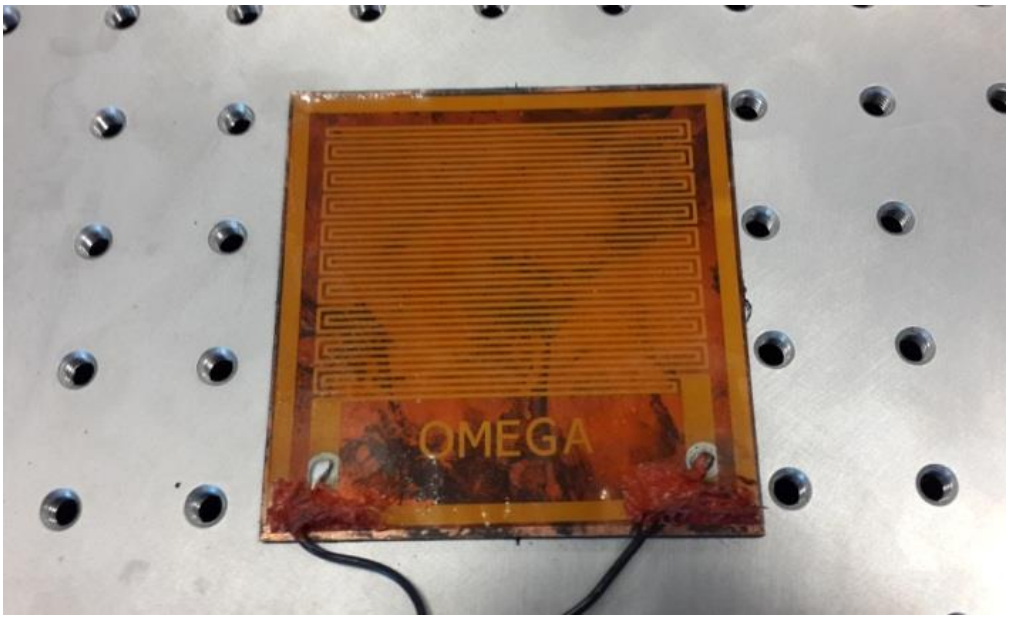

Figure 46: Backside of copper plate

The vertical and horizontal center lines of the front side were 0.5 mm drilled through a CNC-machine. The width for drains was 2 mm. Four thermocouples were placed in the drains in different locations and groves were filled with a heat resistant RTV silicone for a reliable contact between thermocouples and copper, and also more accurate measurement by bringing the rest of the contact surface of the thermocouples to a closer temperature of the copper substrate. Surface of the copper was painted, and the copper plate was fixed vertically by a holder to monitor temperature distribution on the surface through IR camera as seen in Figure 47.

CHAPTER IV

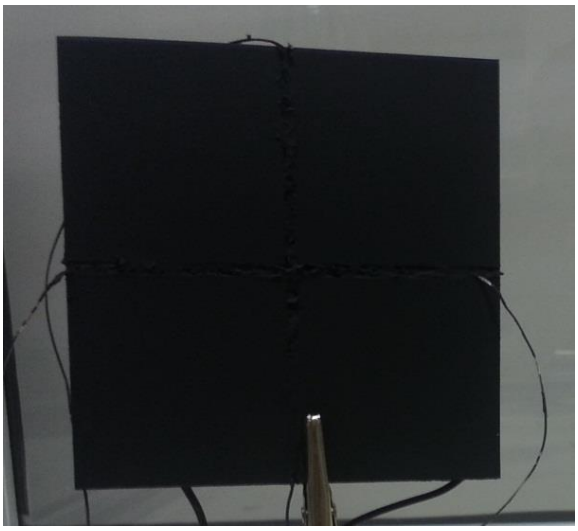

Figure 47: Painted side of copper plate

Copper plate was heated through the flexible heater by using a DC power supply in the thermal test cabinet. After reaching steady state conditions, thermocouple measurements were started to be matched with IR measurements. Emissivity of IR camera was being set to different values. An emissivity of 0.95 was determined to be the emissivity value, which provided same temperature readings for thermocouples and IR camera (Figure 48).

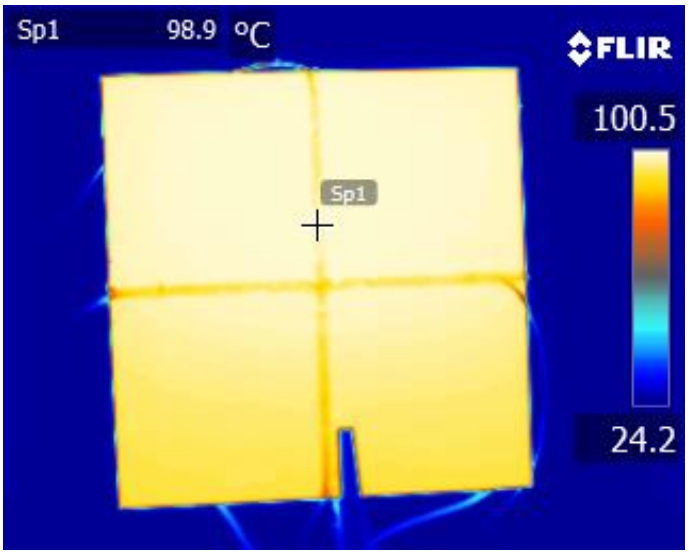

Figure 48: IR image of copper plate

Although a 2 mm-thick and high thermal conductive copper plate was used in this study, small temperature gradients in vertical direction can be observed due to the fact that bottom part of the heater does not involve ohm resistor as seen in Figure 46. Since temperature measurement readings were done on specific points, it was not a fact that affects the accuracy of the results. Emissivity of the paint was determined as 0.95 as the result of the emissivity study.

4.4.1.2. Thermal Conductivity Study

Thermal conductivities of the used materials are very important for the systems with thermal purposes. It is crucial especially for the cooling component of a thermal system such as heat sink. Heat sink of the developed bulb was manufactured with aluminum alloy 6082-T6. Since the manufacturing methods and conditions were not well known for the used material, it was crucial to determine the accurate thermal conductivity of the heat sink, which defines the thermal performance of the system. A thermal conductivity test setup was prepared for a precise determination of the thermal conductivity of the heat sink material. A thin test bar with the dimensions of 6.5 x 1 x 100 mm was manufactured with the aluminum used for heat sink. 1D heat transfer was intended to be observed on this bar by heating it from one side and cooling it from the other side and also by utilizing the facts that the bar is thin, long and high thermal conductive. 1D heat transfer provides an easy and accurate validation of experimental test with computational test. For heating the test bar, two Polyimide heaters (Figure 49) with 15 ohm resistances were attached to both sides of the top part of the test bar to prevent two dimensional conduction heat transfer within the bar. In the next step, test bar and wires were painted with the high heat spray paint with 0.95-emissivity (Figure 50).

CHAPTER IV

Figure 49: Flexible heater

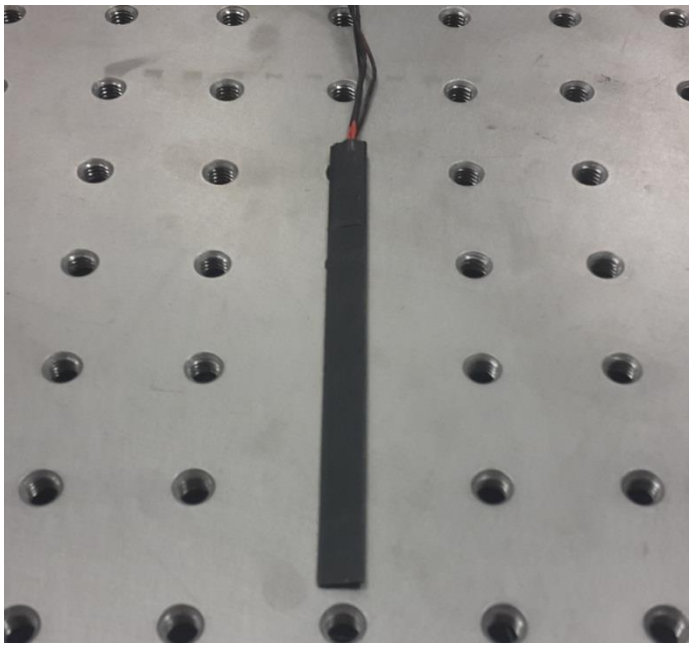

Figure 50: Painted test bar with heaters at both sides of top part

Test bar was hanged on a holder through the wires of heaters. The test bar was immersed 1 cm into cooling water. Cooling water and ambient air were being measured with four thermocouples on different points distinctly away from test bar and each other (Figure 51). Parallel connected heaters were heated by the DC power supply, and it was waited for the system to reach the steady state conditions. Thermocouple measurements were used for determining the time that the steady state conditions were reached. Heater power was varied between 0.1 W and 1 W.

Ambient-, water- and bar temperatures for various heater powers can be seen in Table 10.

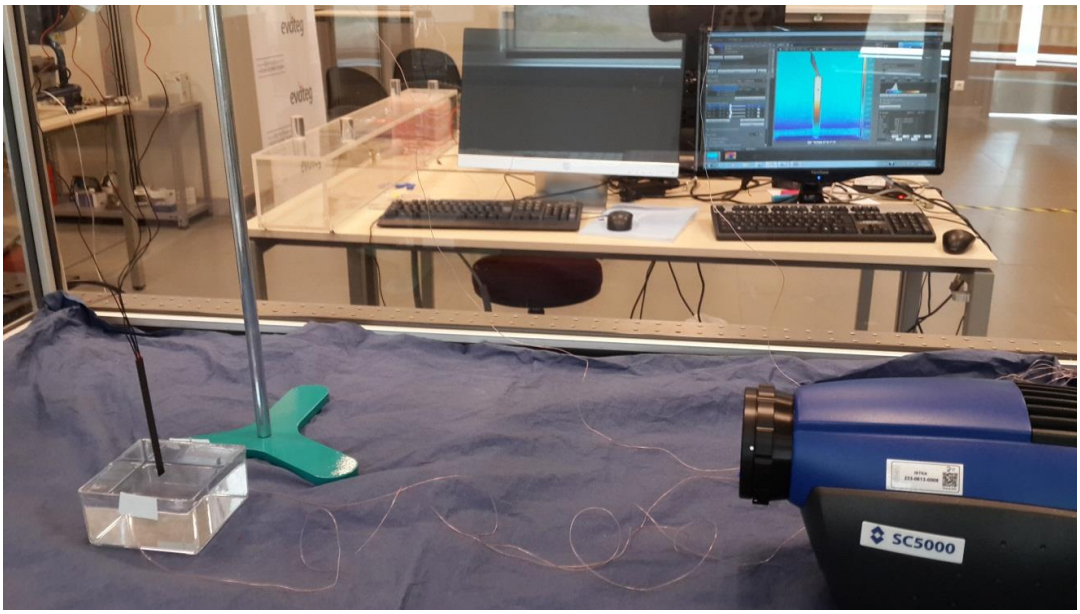

Figure 51: Thermal conductivity test setup

Table 10: Experimental results of thermal conductivity test

Power (W)	T_{Water} (°C)	$T_{Ambient}$ (°C)	T_{max} (°C)
0.1	20.2	23.6	26.7
0.2	20.3	23.6	30.7
0.3	20.4	23.7	34.7
0.4	20.6	23.8	38.4
0.5	20.7	23.8	42.6
0.6	20.9	23.9	46.2
0.7	21.0	23.9	50.0
0.8	21.2	23.9	53.8
0.9	21.3	23.9	57.5
1.0	21.5	24.1	61.3

CFD analysis was carried out for determining the thermal conductivity. Test setup was created carefully in an Icepak model including some part of the heater cables that affect heat transfer. Experimentally obtained varying boundary conditions

occurred based on varying heater powers were simulated for different thermal conductivities of bar. Temperature gradients and velocity vectors for 1 W heater power can be seen in Figure 52 and Figure 53. Temperature results of CFD analysis for the thermal conductivity of 160 W/m-K had the closest trend to by experimental results obtained trend as seen in Figure 54.

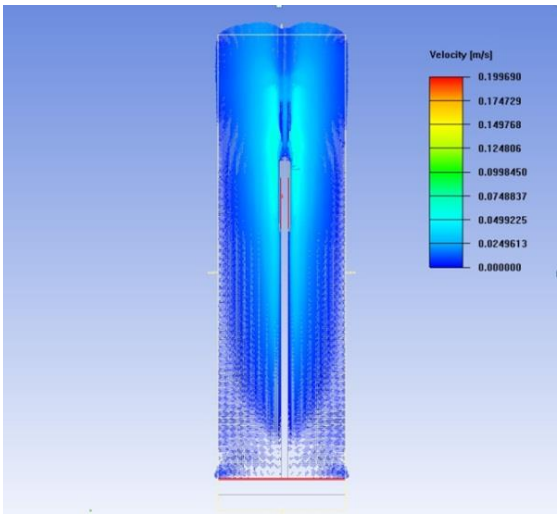

Figure 52: Plane cut vectors for velocity magnitude

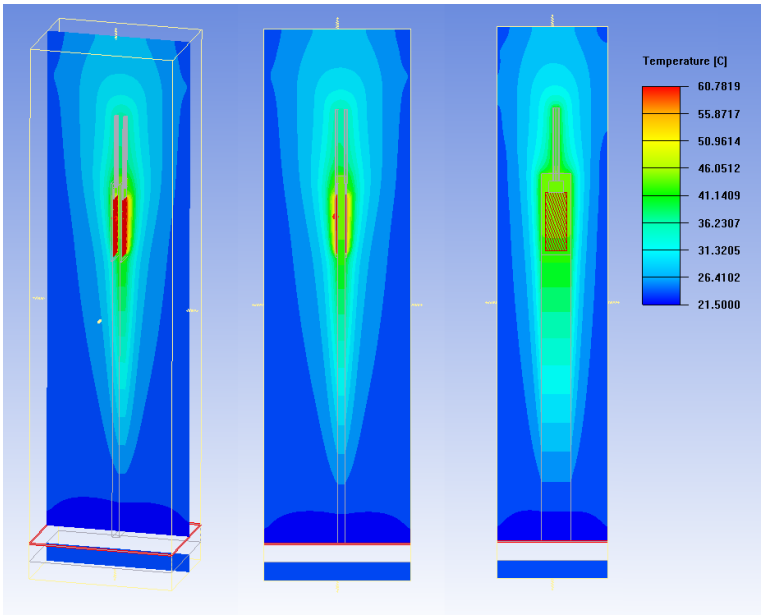

Figure 53: Plane cut contours for temperature

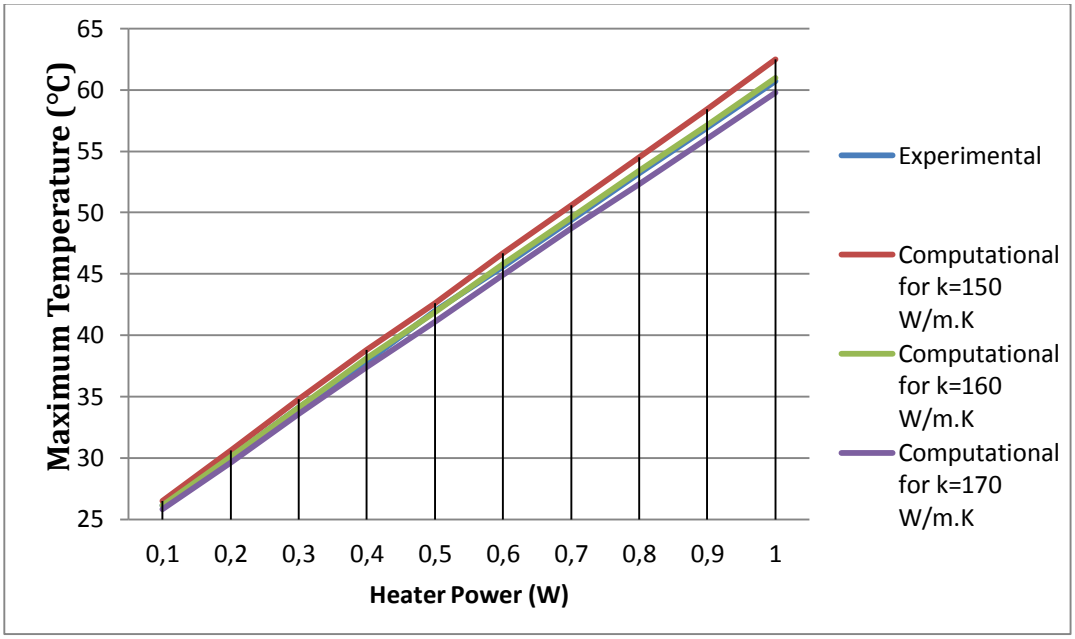

Figure 54: Comparison of experimental results with computational results

Maximum deviation between experimental and computational results for the thermal conductivity of 160 W/m-K was 0.3°C for 10 different heater powers. It was also observed that the trend of CFD results was becoming dissimilar by getting away from 160 W/m-K for thermal conductivity. Maximum temperatures of test sample for thermal conductivities of 150 W/m-K and 170 W/m-K are also represented in Figure 54.

4.4.1.3. Thermal Study of Prototype with Heaters

Thermal test of the developed A19-LED lighting system was carried out by using heaters in thermal conductivity test. Heat sink of the system was manufactured with aluminum alloy 6082-T6 through a 5-axis-CNC machine. Dome for the heater test was produced with PMMA through a 3D printing machine (Figure 55).

CHAPTER IV

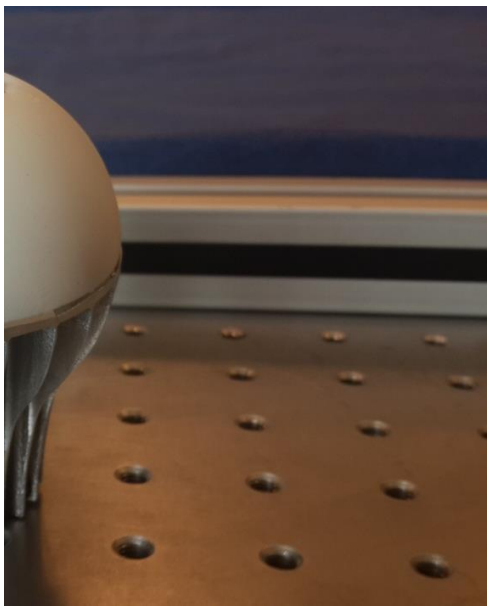

Figure 55: Heat sink with opaque dome

12 Polyimide flexible heaters with 15 ohm resistances were attached to heat sink base and connected to each other in series as seen in Figure 56.

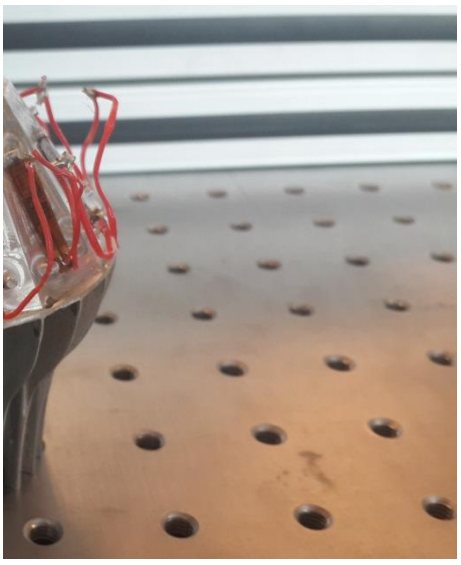

Figure 56: Heat sink with flexible heaters

Dome was attached to heat sink by a heat resistant and easy removable RTV silicone, and a PMMA component was also produced with a 3D printing machine

for filling the driver space. After placing the PMMA component into the space reserved for driver, whole system was painted with the high heat spray paint (Figure 57 and Figure 58).

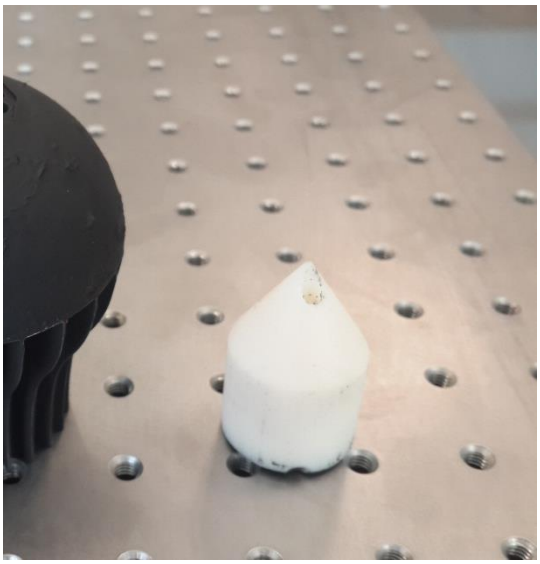

Figure 57: Painted heat sink and space-filling PMMA component

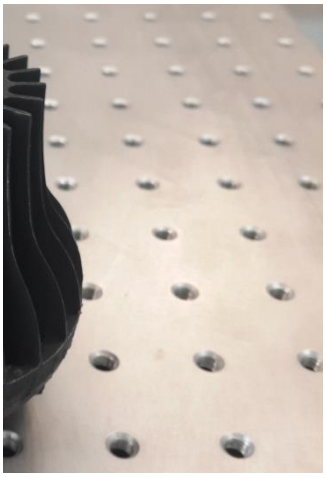

Figure 58: Painted heat sink and space-filling PMMA component

Painted prototype was hanged in the air-tight thermal test setup, which was used in previous thermal studies of commercial bulbs. Heaters were heated with 14 W power through a DC power supply. Ambient air was recorded by using two

distinctly placed T-type thermocouples, and prototype was monitored through the IR camera (Figure 59). IR image of heated prototype under steady state conditions can be seen in Figure 60.

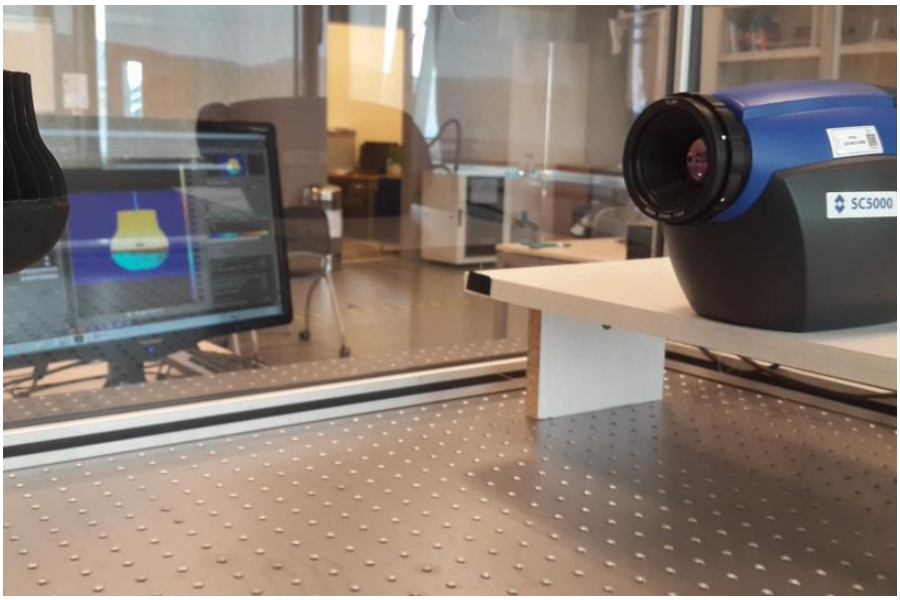

Figure 59: Experimental test setup for prototype with flexible heaters

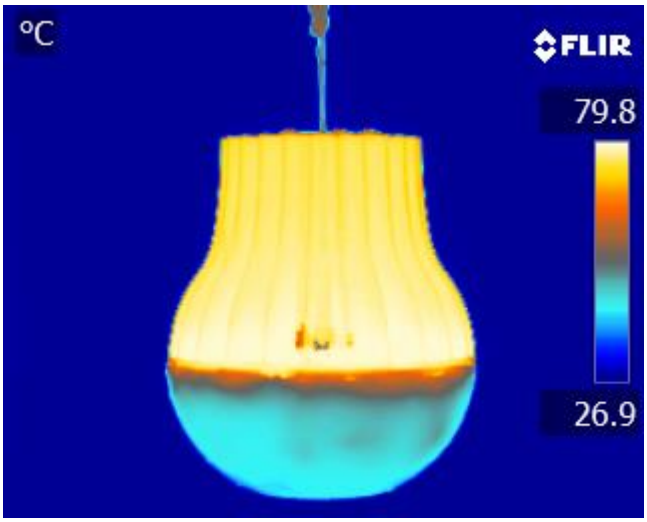

Figure 60: IR image of prototype with heaters

As the result of thermal test, maximum heat sink temperature was found to be 79.8 °C, and 26.6 °C ambient temperature was measured. Difference between

experimental and computational results was 4.9%, which is acceptable. Small geometry differences between CAD model and manufactured prototype can be effective on this deviation. Other important facts can be the errors in thermocouple sensing, data acquisition, IR camera measurements and CFD analysis.

4.4.1.4. Thermal Study of Prototype with LEDs

Manufactured heat sink and test setup was prepared for the second step test, in order to bring them to actual operational conditions of previously tested bulbs and compare it with them. Heaters, opaque PMMA dome, RTV silicone and PMMA space filler from the first experimental test were removed from the heat sink, and the heat sink base was cleaned before mounting PCBs to heat sink base. MCPCBs with CREE XPG-2 LEDs were prepared (Figure 61). Each PCB had three holes, which were located on the rims of each trapezoid heat sink base. One of the PCBs had an extra hole, which matched to the hole on heat sink base for electrical connection of parallel connected PCBs to Edison base. PCBs were mounted on the heat sink base by using a TIM with a thermal conductivity of 0.9 W/m-K.

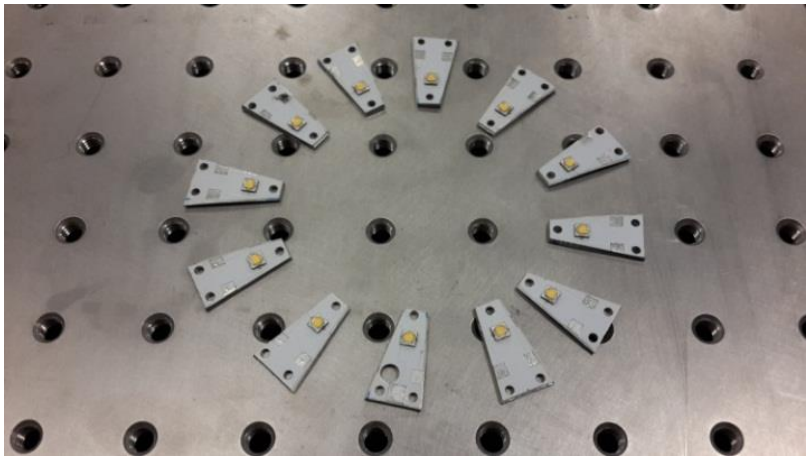

Figure 61: Light engine of prototype

CHAPTER IV

By preparing transparent dome, PMMA was injected into the silicone cast, which was produced based on CAD model. PMMA isolator was produced through a 3D printing machine. Dome, isolator and standard E26 Edison base were attached to heat sink and each other by using a heat resistant epoxy adhesive (Figure 62 and Figure 63).

Figure 62: Prototype for developed lighting system

Figure 63: Prototype for developed lighting system

Prototype was tested in the same thermal test setup and with the same methods of previous thermal tests of commercial LED bulbs (Figure 64). IR image under steady state conditions can be seen in Figure 65.

Figure 64: Experimental test setup for prototype with LEDs

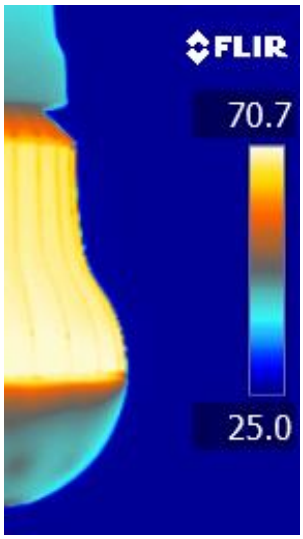

Figure 65: IR image of prototype with heaters

IR camera and thermocouple measurement results show that the maximum heat sink temperature of 70.7 °C was observed for 25 °C ambient temperature, which means a 4 °C/W thermal resistance for 11.3 W heat flow rate. Heat flow rate was determined by the experimental optical test that will be presented in Chapter 4.4.2. Difference between experimental and computational analyses for temperature difference was 3.2%. Thermal resistance under actual conditions was 0.2 °C/W higher than pure thermal performance test, but it has still much better thermal resistance than the best thermal resistance of 5.6 °C/W among the tested bulbs of global vendors.

4.4.2. Optical Studies

Optical studies were carried out through SphereOptics scientific integrating sphere and LMT GO-V 1900 goniophotometer. Optical test setup was prepared as in the optical tests of commercial bulbs (Figure 66). Heat sink temperature and ambient temperatures were monitored through thermocouples. After reaching steady state conditions, results in Table 11 were recorded for an input power of 17.5 W. Integrating sphere used in previous tests of commercial bulbs has a high accuracy, and it was calibrated before measurement as explained in Chapter 3.2.

Table 11: Optical results of prototype

Radiant Flux	6.2 W
Luminous Flux	1817 lm
CCT	3172 K
CRI	82.5

CHAPTER IV

Figure 66: Optical test of prototype in integrating sphere

According to equation (4, heat flow rate of XPG-2 LEDs was 11.3W based on the measured radiant flux of 6.2 W and input power of 17.5 W.

$$\boldsymbol{q = P - \Phi_e} \tag{4}$$

Luminous flux of 1817 lm shows that the goal of 1700 lm was achieved. Low junction temperature due to the high cooling capacity was effective on high luminous flux. CRI value was better than most of the tested bulbs. 3172K of CCT means a warm white light that is also desired for indoor lighting. Although luminous flux, CCT and CRI values were as desired, light distribution of a lighting system is also crucial. For this reason, the prototype was tested in goniophotometer as seen in Figure 67.

Tests were carried out according to IESNA-LM-79-08 [29] scanning resolution requirements of 22.5° lateral and 5° longitudinal grid for typical wide-angle, smooth intensity distributions. Goniometer has a 0.1° accuracy for both axis, and photometer has the accuracy class L (highest accuracy) according to DIN 5032 part

7 [30]. Goniometer was located 10 m away from photometer in a dark room with non-reflective walls, ceiling, floor and curtains (Figure 67). Experimental results can be seen in Figure 68, Figure 69 and Figure 70.

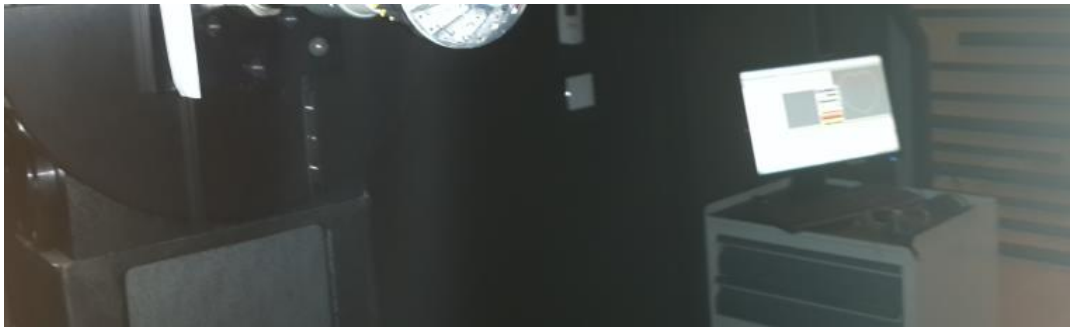

Figure 67: Optical test of prototype by Goniophotometer

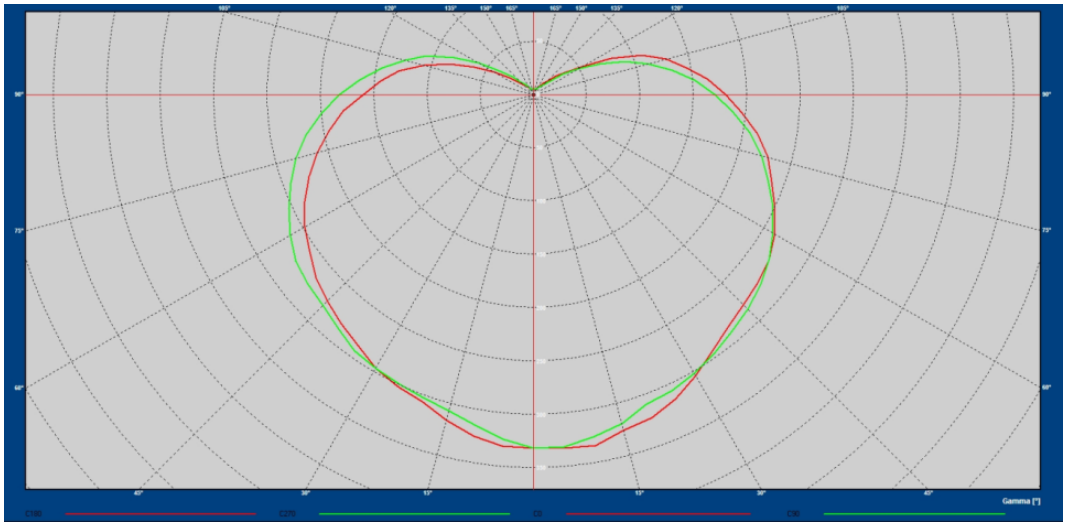

Figure 68: Measured polar diagram of prototype

CHAPTER IV

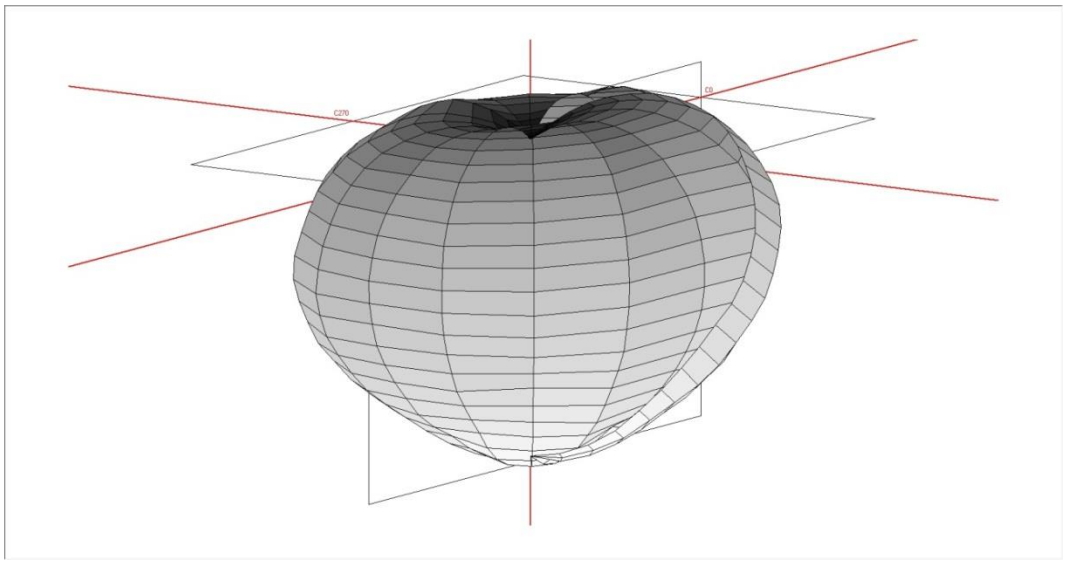

Figure 69: Measured polar diagram of prototype

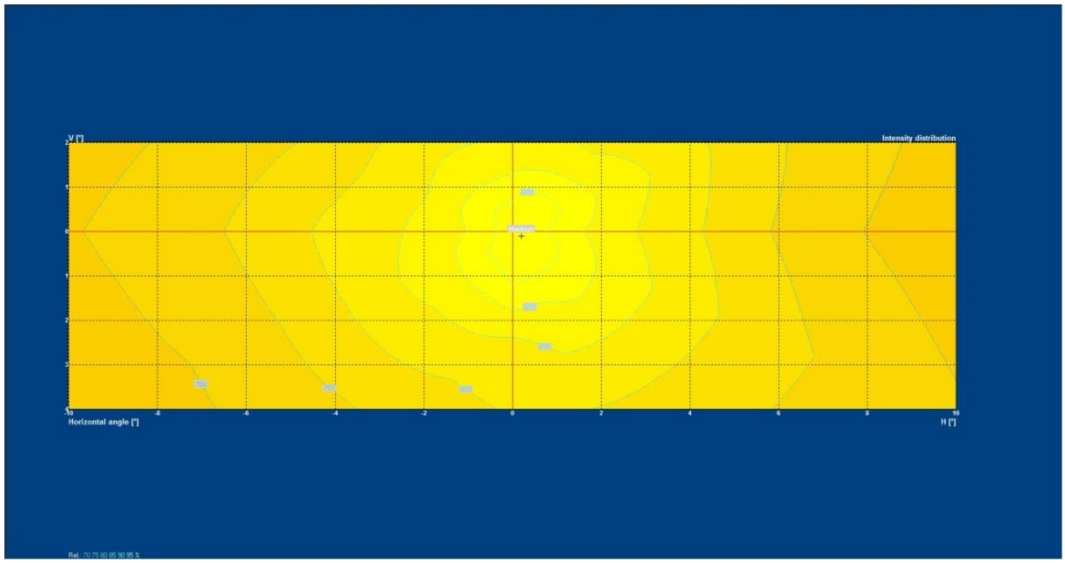

Figure 70: Intensity distribution of prototype

Results show that there was a good agreement between computational and experimental results. Surface properties of dome and small air bubbles in dome were the main reasons for small differences between experimentally and

computationally obtained polar diagrams. In addition to these facts, PCBs were not able to be placed very properly on heat sink base, and LEDs were not smoothly mounted to PCBs. These facts were also very effective on the wavy isolines in Figure 70.

4.5. Optimization

First prototype of new approach provided quite promising results. In this section, a wide-angle intensity distribution bulb is studied computationally. Weaknesses of the first prototype are studied and the thermal design is optimized including electronic driver circuit.

Forward intensity distribution was aimed by the first prototype. Therefore, a design with the preferred heat sink base angle was created that provide a luminous intensity of approximately 350 cd in forward direction. Optical modeling offered useful wide-angle light distributions as seen in Figure 25. A greater angle was preferred for second the prototype with a luminous intensity of approximately 200 cd in forward direction and wide-angle intensity distribution (Figure 71).

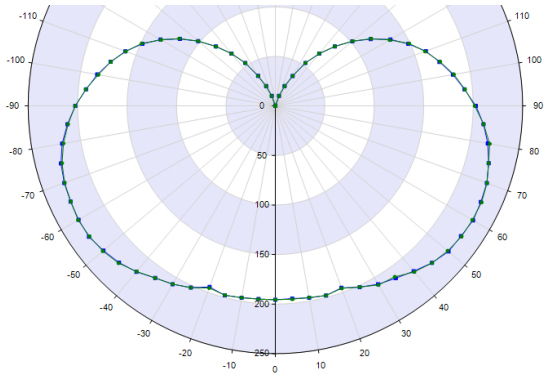

Figure 71: Polar diagram for optimization system

CHAPTER IV

In the analysis of first prototype, it was observed that cooling capacity of the middle section was not efficiently employed, where was actually reserved for cooling of electronic driver circuit. Although the first prototype study was aiming the observation of the thermal and optical performances of the system and the validation between computational and experimental results, optimization should be carried out for the actual conditions. For this reason, electronic driver circuit should be also simulated by the optimization. Since it is not a task of this study to design an electronic driver circuit, it was simulated as a 3D heat source based on estimations. For an input power of 20 W and electronics efficiency of 90%, 2W-heat is generated. Since the required system, electronic components, heat generation rates and positions of the components were unknown; the heat spreader PCB of electronic driver circuit was the heat source in the optimization study. Dimensions were 45 x 22 x 1.6 mm, and heat flow rate was 2 W for MCPCB. The thermal conductivity of MCPCB was defined as 150 W/m-K for CFD analysis.

Design of the lighting system was changed by the optimization due to the determined optical purposes and enhancement opportunity for thermal performance based on mass. Heat sink base angle was increased by the prototype-2, first of all for optical purposes. Increasing the heat sink base angle was expected to bring also some thermal advantageous. These were better matching of heat sink base and fins with natural convection flow direction, larger air inlet size and minimizing the dome volume. Prototype-1 had a flow guide in the middle part of the heat sink with a large angle. This was so designed that natural convection flows did not undergo any large angle changes in their development direction by passing through the

middle section of the heat sink. Flow guide angle with horizontal axis was also reduced in the prototype 2, and it was still expected to bring some advantages. First advantage was the less material requirement and less weight. Smaller angle was also expected to bring a less thermal resistance between flow guide and electronic driver circuit due to the reduced interface material in between, which enhances the thermal management performance of electronic driver circuit. Thermal connection between fins and electronic driver circuit was expected to become weaker that can have positive or negative effects for cooling of driver and whole system.

By the optimization system, fin length was also varied, which also changed the fin spacing due to 3D geometry of the fin structure. But some fins were very limited for changing their length, since they lose their mechanical connection by some of the variations of length. For this reason, fin number was reduced to half in the optimization system. This reduction had several advantages and some disadvantages. By reducing the fin number too dense fin structure was removed and a wide range of optimization was provided. This may have a negative impact on total cooling capacity as a disadvantage due to the reduced heat transfer area. However, it was not expected to bring remarkable thermal performance drop. Since there was still sufficient thermal path through fins, and electronic driver circuit was placed on the other side of the fins as another heat source. Since thermal connection between LEDs and middle section was weaker with a less number of fins, it was expected that cooling capacity of middle section was employed rather for electronic driver circuit. Weight and surface area of the system were hereby decreased, and it was expected to enhance the thermal performance based on mass

and surface area. Smaller surface area in prototype-2 can decrease heat transfer rate by thermal radiation. But there can be some benefits for the efficiency based on surface area. Fin surfaces targeted surrounding area better due to 3D structure of fins, and there were fewer fins, which face each other and absorb the thermal radiation emitted by each other. Optimum fin number could be also studied for the highest heat removal by thermal radiation. But it was not a research interest in this study, since the natural convection had the priority as the main cooling mechanism. Decreasing the fin number also means a less fin resistance to natural convection flows and stronger natural convection flows.

Heat transfer coefficient for natural convection was expected to be increased, since the thermal resistance was expected to be less for a smaller surface area. Only expected disadvantage was the weaker thermal connection between LEDs and the rest of the heat sink, which means a better cooling of electronic driver circuit. Due to the facts that capacitors of an electronic driver circuit is the lowest rated part, and high heat flux is existent on driver components, electronic driver circuit had the primary priority in this study. LEDs were already in safe and efficient temperature region in all cases of this study. So it is based on the priorities of the researcher, if junction temperature of LEDs allowed to be higher. Heat sinks used for prototype-1 and optimization can be seen in Figure 72.

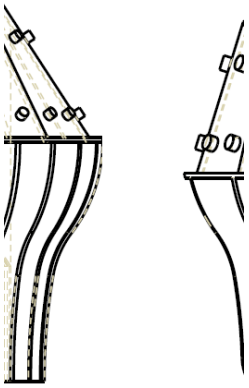

Figure 72: Comparison between heat sinks of prototypes

Structures of dome and heat sink base were changed by increasing the heat sink base angle. Total volume reserved for the dome was decreased, and this resulted with the increment of the cooling volume inside heat sink. Dome structure was also changed so that it allowed a wide-angle luminous intensity distribution. Heat sink became similar to advantageous vertical heat sinks that match natural convection development direction better. Heat transfer area of PCBs and heat sink base were increased. CAD model of prototype-2 can be seen in Figure 73.

Figure 73: CAD model of prototype-2

Material properties and boundary conditions were same as in the CFD analysis of prototype-1 with LEDs. Additional input power of 2 W was defined for driver. 54 analyses were carried out with varying heat sink base thicknesses between 1 and 1.5 mm, varying fin thicknesses between 1 and 1.5 mm, and varying fin lengths between 18 and 28 mm. Fin length of 20 mm can be seen in Figure 74. Boundary conditions, material and mesh properties of CFD analysis with LEDs were also same for the optimization. Mesh number was varying between 1,446,300 and 1,514,556 for 54 different cases. Detailed CFD results can be seen Table 12. In Table 12 given surface area is the total surface area of the whole heat sink, while the surface area exposed to ambient air will be used by FOM calculations in Chapter 5. Mass of the heat sink was calculated by multiplying the volume by approximate density of 2700 kg/m^3 for aluminum.

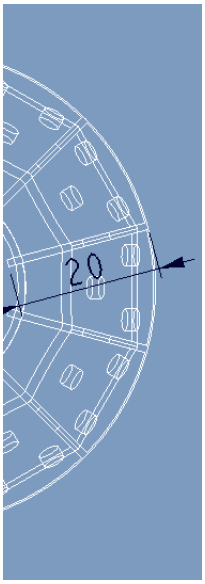

Figure 74: Heat sink with 20 mm fin length

Table 12: Optimization results

t_b (µm)	t_f (µm)	l_f (mm)	T_{hs_max} (°C)	T_{hs_min} (°C)	T_{hs_mean} (°C)	T_{driver} (°C)	T_j (°C)	m_{hs} (g)	A_{hs} (m^2)
100	100	18	67.4	63	65.1	83.3	77.8	49.2	0.0372
100	100	20	66.3	61.6	64.1	83.2	77.1	52.5	0.0396
100	100	22	65.4	60.4	63.3	82.9	76.1	55.9	0.0421
100	100	24	65.1	61	63.1	82.9	75.3	59.3	0.0447
100	100	26	65.4	60.5	63.5	83.4	75.9	62.8	0.0472
100	100	28	66	61.6	64.1	83.9	76.3	66.2	0.0498
100	125	18	67.1	62.9	65	83.5	77.4	55.5	0.0373
100	125	20	66	62	64	83.2	76.3	59.5	0.0397
100	125	22	65.4	60.4	63.5	83.1	76.1	63.8	0.0423
100	125	24	65.2	61.1	63.4	83.3	75.4	68.1	0.0448
100	125	26	65.6	60.8	63.8	83.8	76.1	72.4	0.0474
100	125	28	66.4	62	64.6	84.4	76.7	76.6	0.0499
100	150	18	66.7	63	64.7	83.5	77	61.7	0.0374
100	150	20	65.9	61.1	64	83.5	76.8	66.5	0.0398
100	150	22	65.2	60.3	63.4	83.2	75.9	71.7	0.0424
100	150	24	65.2	61.1	63.4	83.4	75.3	76.8	0.0449
100	150	26	66	61.4	64.3	84.6	76.5	82.0	0.0475
100	150	28	66.5	62.2	64.9	84.7	76.8	87.1	0.05
125	100	18	67.4	63.2	65.3	83.5	77.8	52.6	0.037
125	100	20	66.2	62.4	64.2	83.2	76.6	55.8	0.0395
125	100	22	65.4	60.6	63.5	83	76.2	59.2	0.042
125	100	24	65.1	61.3	63.4	83.1	75.4	62.7	0.0445
125	100	26	65.4	60.9	63.7	83.7	76	66.1	0.0471
125	100	28	66	61.9	64.3	84.1	76.4	69.5	0.0496
125	125	18	67.1	63.2	65.2	83.7	77.5	58.7	0.0372
125	125	20	66	62.3	64.2	83.4	76.4	62.8	0.0396

t_b (µm)	t_f (µm)	l_f (mm)	T_{hs_max} (°C)	T_{hs_min} (°C)	T_{hs_mean} (°C)	T_{driver} (°C)	T_j (°C)	m_{hs} (g)	A_{hs} (m^2)
125	125	22	65.4	60.7	63.7	83.3	76.1	67.0	0.0421
125	125	24	65.3	61.5	63.7	83.5	75.6	71.3	0.0447
125	125	26	65.6	61.1	64.1	84.1	76.2	75.6	0.0472
125	125	28	66.4	62.2	64.8	84.6	76.7	79.9	0.0497
125	150	18	66.8	63.2	65	83.7	77.1	64.9	0.0373
125	150	20	65.8	62	64.1	83.5	76.1	69.7	0.0397
125	150	22	65.2	60.5	63.6	83.4	75.9	74.9	0.0422
125	150	24	65.2	61.4	63.7	83.6	75.4	80.0	0.0448
125	150	26	65.8	61.2	64.3	84.3	76.3	85.2	0.0473
125	150	28	66.6	62.5	65.1	85	76.9	90.3	0.0499
150	100	18	67.6	63.4	65.5	83.7	77.9	55.9	0.0369
150	100	20	66.3	62.7	64.5	83.4	76.7	59.1	0.0393
150	100	22	65.4	60.8	63.7	83.2	76.2	62.5	0.0418
150	100	24	65.2	61.5	63.6	83.3	75.5	66.0	0.0444
150	100	26	65.5	61.1	63.9	83.8	75.8	69.4	0.0469
150	100	28	66.1	62.2	64.6	84.4	76.5	72.8	0.0495
150	125	18	67.2	63.4	65.4	83.9	77.6	62.0	0.037
150	125	20	66.1	62.6	64.5	83.6	76.5	66.0	0.0394
150	125	22	65.4	60.9	63.9	83.5	76.2	70.3	0.042
150	125	24	65.3	61.7	63.8	83.6	75.6	74.6	0.0445
150	125	26	65.7	61.4	64.3	84.2	76.1	78.9	0.0471
150	125	28	66.5	62.5	65	84.8	76.8	83.1	0.0496
150	150	18	66.8	63.5	65.2	83.9	77.2	68.0	0.0371
150	150	20	66.1	62.5	64.6	84.1	76.5	66.0	0.0395
150	150	22	65.3	60.8	63.8	83.6	76.1	78.0	0.0421
150	150	24	65.3	61.7	63.9	83.9	75.5	83.2	0.0446
150	150	26	66.2	62	64.8	85	76.7	88.3	0.0472
150	150	28	66.6	62.7	65.3	85.1	77	93.5	0.0497

CHAPTER IV

Results show that base thickness does not have a significant effect on thermal resistance in the optimization range, since heat is effectively spread on heat sink base. Highest difference for varying base thicknesses was 0.3 °C and observed for fin thickness of 150 mm and fin number of 20. Increasing the base thickness was sometimes advantageous and sometime disadvantageous due to its effect on the natural convection development and heat sink efficiency.

Tight interaction between optimization parameters can be observed on the results. For instance, results showed that increasing fin thickness enhanced the thermal connection and provided a better heat transfer between middle section of heat sink and LEDs for short fin lengths. This provided a better cooling for LEDs, while generated heat by LEDs are better conducted within heat sink. It also meant less cooling capacity and worse thermal performance for electronic driver circuit. Fin length optimization for 1 mm base thickness can be seen in Figure 75.

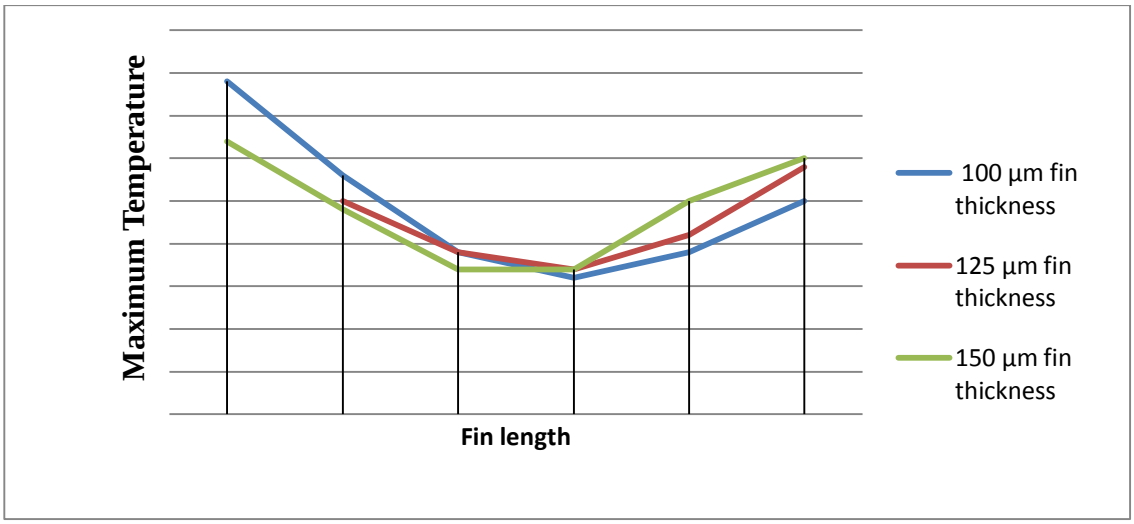

Figure 75: Fin length optimization for 1 mm base thickness

Figure 75 shows that thick fins are beneficial for small fin lengths. By the higher fin lengths, minimum fin spacing becomes shorter due to 3D geometry of fin structure and thin fins become advantageous. This trend can be also observed for different base thickness.

Element number was 1,446,999 for the mesh of the optimum heat sink as seen in Figure 76. Maximum heat sink temperature for various mesh structures can be seen in Figure 77. CFD results of the optimum system can be seen in Figure 78, Figure 79, Figure 80, Figure 81, Figure 82, Figure 83 and Figure 84.

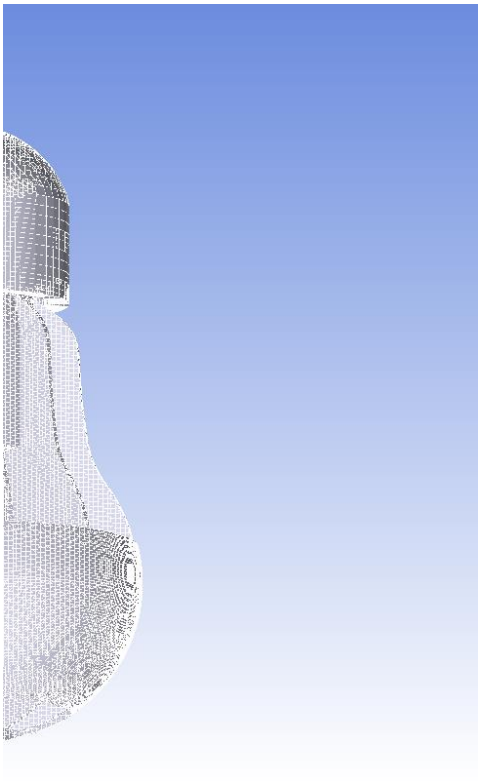

Figure 76: Mesh visualization

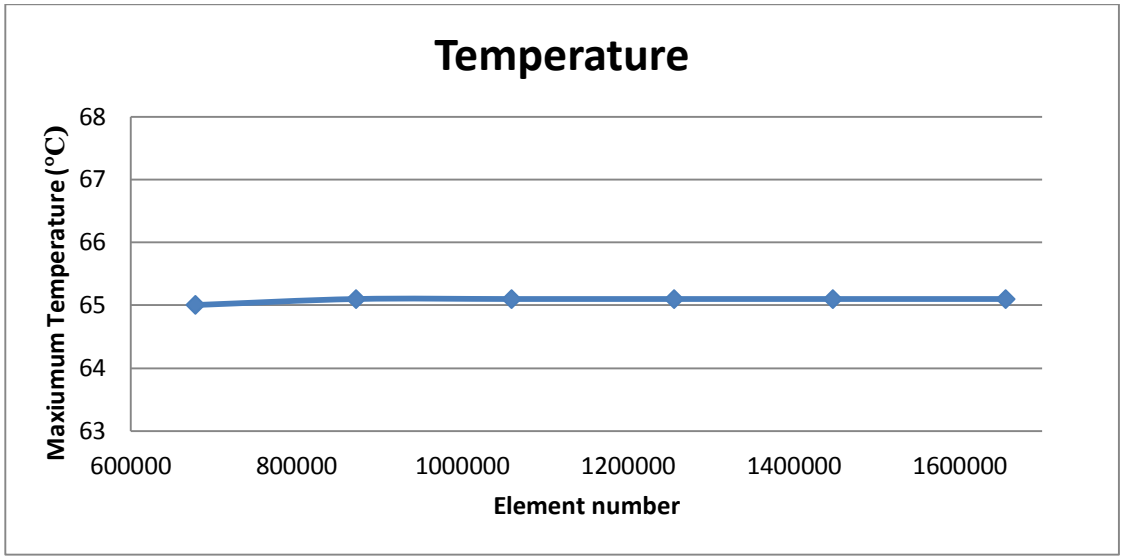

Figure 77: Maximum heat sink temperature for various mesh structures

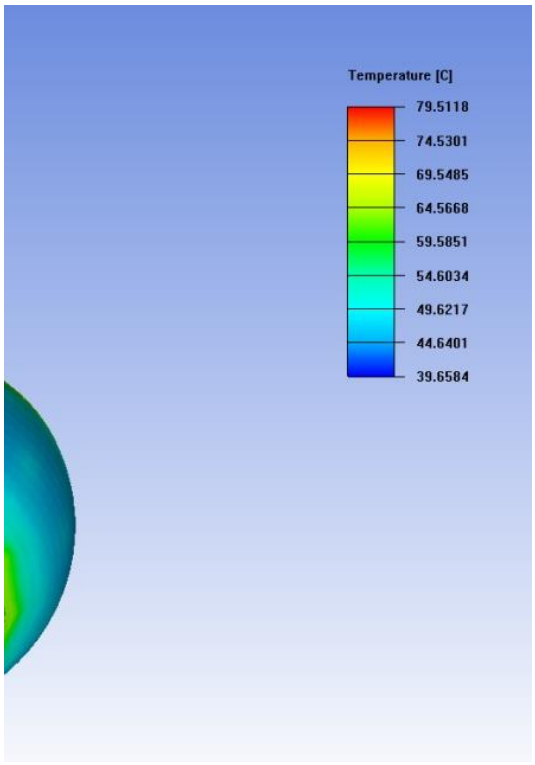

Figure 78: Temperature contours on optimized system

CHAPTER IV

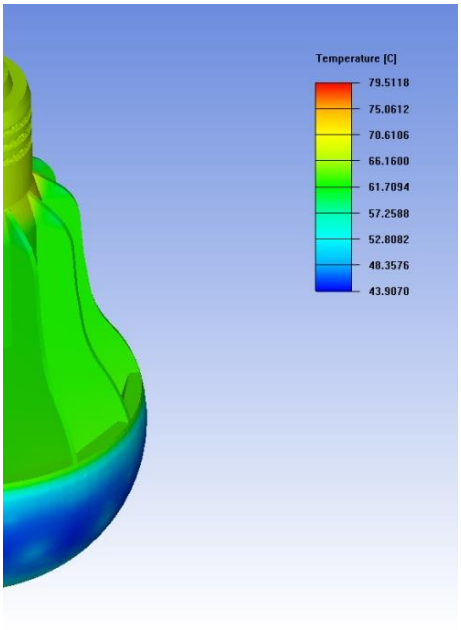

Figure 79: Temperature contours on optimized system

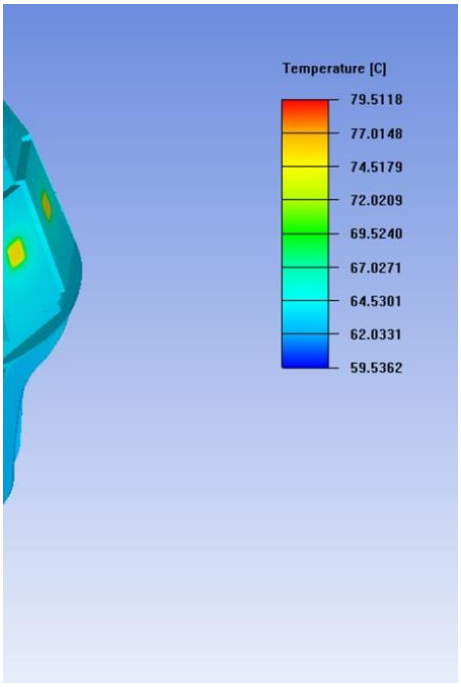

Figure 80: Temperature contours on optimized system

CHAPTER IV

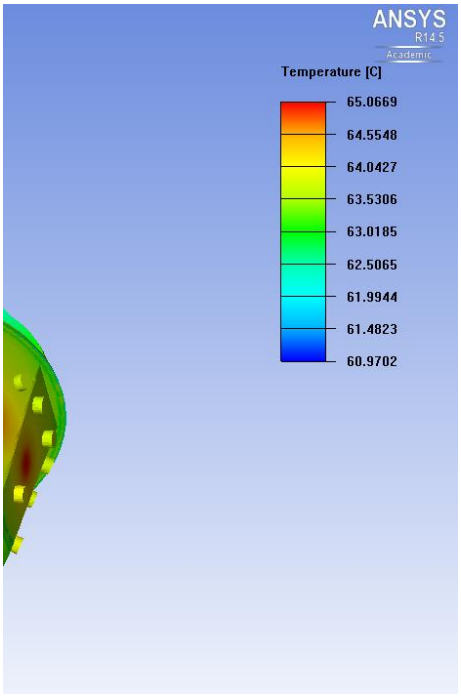

Figure 81: Temperature contours on optimized system

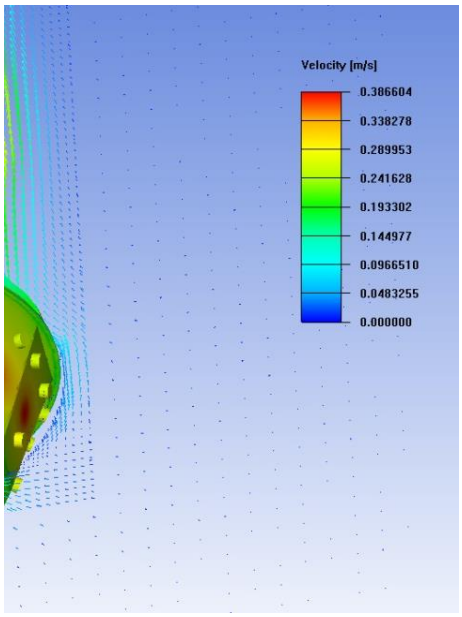

Figure 82: Temperature contours and velocity vectors

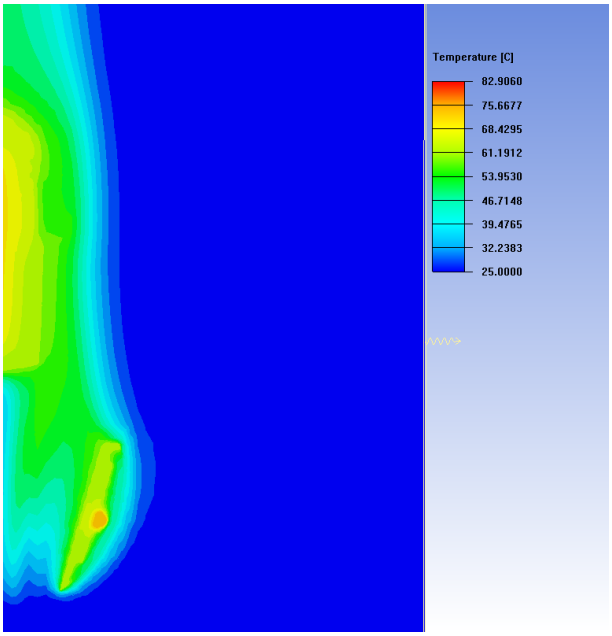

Figure 83: Plane cut contours for temperature (in the center of the system)

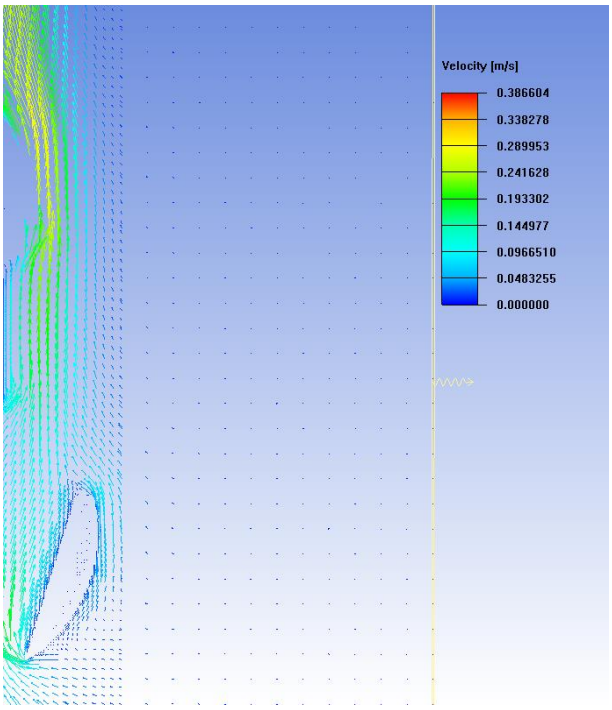

Figure 84: Plane cut vectors for velocity magnitude (in the center of the system)

Temperature contours in Figure 78 and Figure 79 show that there are warmer areas on dome, since LEDs are close to dome. Results indicate the meaning of the highest priority for cooling of electronic driver circuit, which has the highest temperature in the system with 82.9 °C. The junction temperature of 75.3 °C was achieved for idealized thermal path between heat sink base and LEDs. Gap between heat sink base and MCPCB (k = 150 W/m-K) was assumed as 0.2 mm, which was filled with the same TIM (k = 0.9 W/m-K) used in the analysis of prototype-1. Under actual conditions assembly of heat sink base, TIM, PCB and LEDs may not be as precise as assumed here. Another important point is that thermal resistance between heat sink and heat sources (LEDs and electronic circuit driver) was not optimized based on advanced thermal materials, mounting technologies and methods but only on system parameters. Package level thermal management of LEDs and board level thermal management of LEDs and electronic driver circuit based on referred areas were not any research fields in this study.

Highest heat sink temperature was obtained as 65.1 °C for 13.3 W total power (2 W higher total power compared to CFD analysis of prototype-1). A 4.1 °C temperature difference within heat sink is still less than by prototype-1 obtained temperature difference (4.4 °C by CFD result), although the total power is higher. Difference between highest heat sink temperature and mean heat sink temperature was 2 °C this time, which is 0.1 °C less compared to prototype-1 with less heat generation. These results indicate a lower thermal resistance for heat conduction and much better heat dissipation, although fin number was reduced to half. This can also be explained by the use of driver as another heat source in the critical part of the heat sink that increases the efficiency.

By CFD optimization obtained thermal resistance of 3 °C/W is much better than experimentally obtained thermal resistances of 5.6 °C/W for bulb-A with the highest thermal performance among the tested bulbs and 4.0 °C/W for the manufactured prototype. Prototype-2 is also expected to have a superior performance by the

experimental test, when the fact is considered that the highest difference between computational and experimental results was 4.9% in this study, although there were small differences between the CAD model and the manufactured prototype.

Heat sink surface area exposed to ambient air was 530 cm^3 for prototype-1 and 311 cm^3 for prototype-2. Surface areas of both prototypes are much larger than tested commercial A-line bulbs. This shows the advantage of the new approach for having a larger surface area for the same volume. Thermal resistance of prototype-2 was less than the thermal resistance of prototype-1, although surface area was 41.3 % reduced. This can be explained by the increased heat sink efficiency and heat transfer coefficients of the system.

Mass of prototype-1 was experimentally measured as 129.4 g without driver. Mass of an adequate electronic driver circuit with 500 mA and 35 V output in Figure 85 (17.6 g) and TIM mass (15.5 g based on the CAD model) between heat sink and electronic circuit driver were also taken into account for the total mass of prototype-1 (162.5g). TIM mass was calculated by using the density of gap filler material based on the CAD model. For calculating the mass of second prototype, densities of dome material and isolation material are calculated by measuring the mass of the components from prototype-1 experimentally and using CAD models. Total mass of prototype-2 was calculated as 101.1 g (adhesives and wires are neglected). This shows the important mass reduction of the optimized prototype. The total mass of main components for the optimized prototype is also much smaller than the tested commercial A-line bulbs.

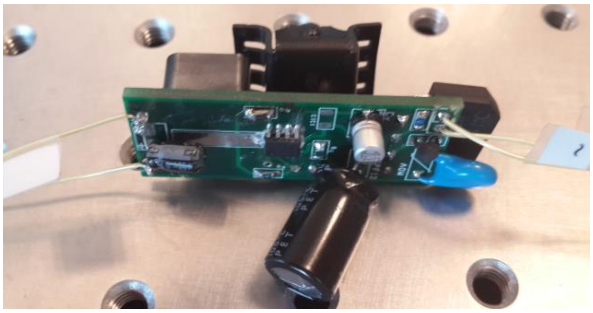

Figure 85: A19 electronic driver circuit

CHAPTER IV

Results show that developed prototypes have better performances based on various performance metrics. Enhanced thermal performance of prototype-2 despite the reduction in mass and surface area indicates the total system optimization, which was aimed by this study.

CHAPTER V

DEVELOPMENT OF FIGURE OF MERITS FOR SSL SYSTEMS [11]

LED systems require a cross-functional research including thermal management, LEDs, materials, packaging, optical, mechanical and electrical designs. Therefore, bringing different functions to the same ground requires a compact design presentation approach that can be met by developing figure of merits (FOMs). Therefore, in this chapter a number of FOMs will be proposed. Test results of commercial A-line bulbs and developed prototypes will be analyzed and compared with each other by using proposed FOMs.

Complexity of combining various design perspectives with the development of new approaches for LED lamps is also related to the advancement in production technology development. Since multi-task design of various engineering fields is rather complicated, it is not sufficient to evaluate the LED lamps with the limited parameters such as standalone thermal, optical or electrical. In order to prevent the confusion, new FOMs are required to be developed for the multi-aspect performance analysis of LED lamps. This study offers several FOMs to enable the interpretation for the desired issues. Thermal and optical experimental test results of commercial A-line LED bulbs are presented based on the FOMs with a composition of different design approaches. Beyond the designers and engineers, proposed FOMs also attempt to clarify consumer's confusion for the thermal side directly related to reliability and lifetime by a combination of it with optical, electrical, geometric and weight parameters.

FOMs are produced through the analysis of the experimental results based on thermal resistance, luminous efficacy, opto-thermal resistance and multi-aspect performances. These FOMs are presented in Table 13 to provide a common perspective for researchers and consumers.

CHAPTER V

Table 13: Proposed combinations of FOMs

FOM	Formula	Unit	Description
FOM_R	$\Delta T/q$	K/W	Thermal resistance
$FOM_{R,m}$	ΔT-m/q	K-kg/W	Thermal resistance based on mass
$FOM_{R,A}$	ΔT-A/q	K-cm²/W	Thermal resistance based on surface area
$FOM_{R,m,A}$	ΔT-m-A/q	K-kg-cm²/W	Thermal resistance based on mass and surface area
FOM_{LPW}	Φ/P	lm/W	Luminous efficacy
$FOM_{LPW,m}$	Φ/P-m	lm/W-kg	Luminous efficacy based on mass
$FOM_{LPW,A}$	Φ/P-A	lm/W-cm²	Luminous efficacy based on surface area
$FOM_{LPW,m,A}$	Φ/P-m-A	lm/W-kg-cm²	Luminous efficacy based on mass and surface area
$FOM_{T,L}$	$\Delta T/\Phi$	K/lm	Opto-thermal resistance
$FOM_{T,m,L}$	ΔT-m/Φ	K-kg/lm	Opto-thermal resistance based on mass
$FOM_{T,A,L}$	ΔT-A/Φ	K-cm²/lm	Opto-thermal resistance based on surface area
$FOM_{T,m,A,L}$	ΔT-m-A/Φ	K-kg-cm²/lm	Opto-thermal resistance based on mass and surface area

Thermal resistance is one the most critical parameters to evaluate the thermal performance of a cooling system. It is important to know the amount of heat that heat sink is capable of removing per surface area. It is usually assumed that a heat sink with a very intricate surface needs a long process to be manufactured. Low thermal resistance alone may not be enough for preferring a specific heat sink because of the unacceptable time and energy consumption required for manufacturing or the manufacturing capability requirements. Target is the maximum heat removal with the simplest heat sink design and the lowest amount of material. From consumer's point of view, low weight is primarily preferred, since they are used to have low or no-weight products of traditional lighting technologies. Risk of injury by falling down of a ceiling lamp is another fact that needs to be considered in lighting systems.

Derivations of this study are produced based on the mass of LED lamps and surface

area of heat sinks. $FOM_{R,m}$ represents the product of the thermal resistance and the mass of bulb. $FOM_{R,A}$ represents the product of the thermal resistance and the surface area of heat sink, that indicates how efficiently a heat sink removes heat to ambient air based on surface area. While most of the heat is through heat sink removed, it is practical to analyze the heat dissipation based on surface area of heat sink. $FOM_{R,m,A}$ is the final product of the thermal resistance, mass and surface area. Basic thermal resistance calculation used for the performance analysis of the tested bulbs is;

$$\boldsymbol{R = \frac{T_{max} - T_a}{q}} \tag{5}$$

where T_{max} is the maximum heat sink surface temperature measured with IR camera, T_{amb} is the ambient temperature measured with thermocouples and q is the heat flow rate calculated as shown in (4). Comparison of tested bulbs and prototypes based on the derivations of thermal resistance can be seen in Figure 86 and Figure 87 (Experimental results for prototype-1 and computational results for prototype-2).

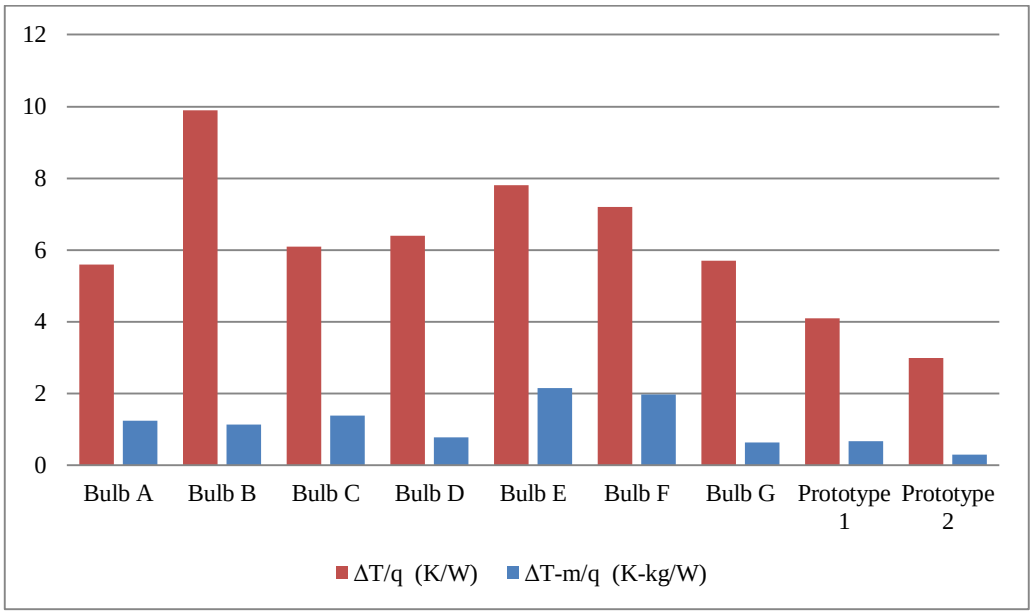

Figure 86: Variation of FOM_R and $FOM_{R,m}$ for various lamps

CHAPTER V

Bulb-B has the highest thermal resistance among the commercial bulbs as seen in Figure 86 due to its small heat sink. Bulb-F indicates a decrease in thermal resistance with the increasing input power compared to bulb-E. Not only different LEDs and electronics components enhance the thermal performance, but also increasing surface temperature of a heat sink simply increases the heat transfer coefficients and enhances the thermal performance. Bulb-A with a high heat sink temperature and effective cooling design has the lowest thermal resistance among the commercial bulbs. Bulb-G follows bulb-A based on thermal resistance. Bulb-G and bulb-D have the best results due to the thermal resistance based on mass among the commercial bulbs. This shows the effective heat removal of simple heat sink with large surface area and light-weight external finned heat sink. Bulb-E and bulb-F with liquid cooling have the worst results on this perspective because of the large weight caused by liquid inside. Despite the fact that bulb-E and bulb-F have both high thermal resistances and mass based thermal resistances, liquid inside the dome prevents the hot spots on LEDs which is important for reliability. Heat transfer in dome direction is another benefit of liquid cooling inside the dome. Prototype-2 has the lowest thermal resistance and the lowest thermal resistance based on mass. Thermal resistance of prototype-1 is also less than all tested commercial bulbs. Thermal resistances based on mass of prototype-1 and bulb-G are almost same.

CHAPTER V

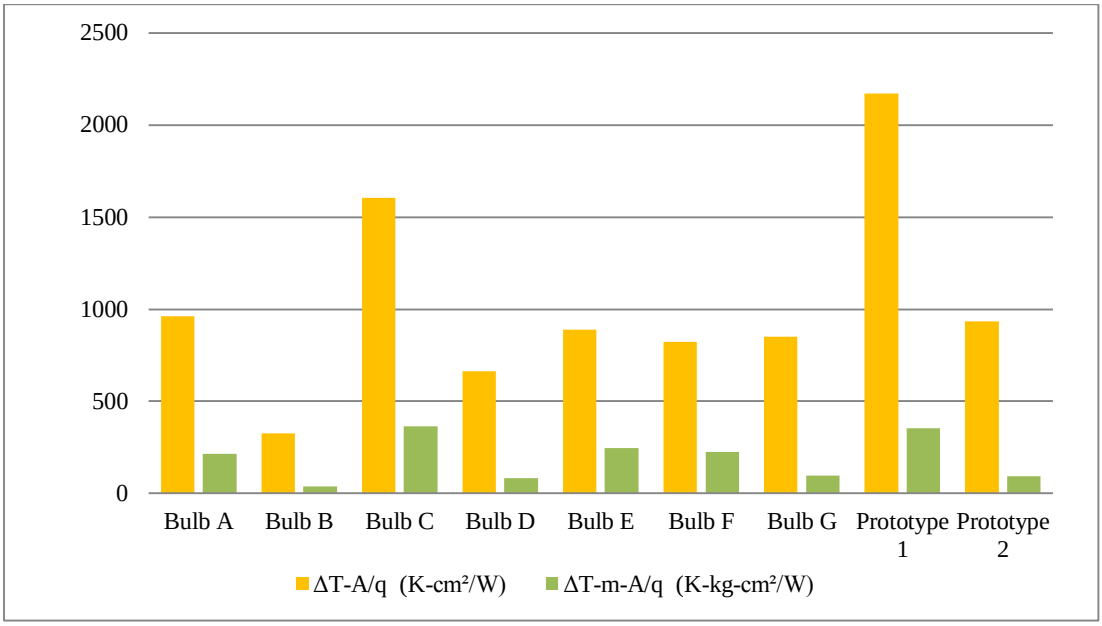

Figure 87: Variation of $FOM_{R,A}$ and $FOM_{R,m,A}$ for various lamps

Due to the results based on $FOM_{R,A}$ (see Figure 87), bulb-B with the very high surface temperature and smallest surface area is the most advantageous one. This shows the effective heat removal based on surface area despite the high thermal resistance. If the system is still operational with a high junction temperature, it can be advantageous to use a small and cheap heat sink and increase its efficiency. Bulb-C has the poorest performance among the commercial bulbs due to its large surface area inside the dome. Since most of the heat sink is inside the dome, heat transfer coefficients are not as high as observed by the other bulbs. Complex heat sink and system structure of bulb-C shows that it is not easily manufacturable. Low heat sink surface emissivity is a reason that as a complete system effectively cooled bulb-A has a high thermal resistance based on surface area. Bulb-B with the highest thermal resistance is again the most advantageous one, when both surface area and mass are taken into consideration. Bulb-D and bulb-G have satisfactory performances based on $FOM_{R,m,A}$. Bulb-B, bulb-D and bulb-G with the best combined performances based on thermal

resistance are the ones which are easy to manufacture as well. Thermal resistance of prototype-1 based on surface area is higher than the thermal resistances of any other bulbs, which may also be seen as a benefit for this special case of new approach, since it has a large surface area and it can be easily manufactured at the same time. Thermal performance of prototype-2 is similar to commercial bulbs and it is advantageous, when both mass and surface are taken into account.

Luminous efficacy is a very useful parameter that indicates total system efficacy including optics and electronics, which is defined as

$$\boldsymbol{LPW = \frac{\Phi}{P}} \tag{6}$$

where Φ represents luminous flux and P is input power of LED bulb. New FOMs are also produced by the production of luminous efficacy with the inverse of mass and surface area again similar to the FOMs based on thermal resistance. $FOM_{LPW,m}$ shows how much lumen is produced per 1 W input power and 1 kg bulb mass, and $FOM_{LPW,A}$ shows the efficacy per 1 cm² surface area of heat sink instead of 1 kg bulb mass. For a combined efficacy analysis, $FOM_{LPW,m,A}$ is the ratio of luminous flux to the product of input power, mass and surface area. Luminous efficacy and other system efficacies based on mass and surface area are represented in Figure 88 and Figure 89. Prototypes will not be compared by the rest of the FOMs, since prototypes do not have any drivers that decrease LPW. Experimentally obtained LPW of prototype-1 was 103.8, which is much higher than the values obtained by commercial bulbs. Prototypes will still not be included in the analysis of next FOMs, since the referred reason complicate a correct comparison.

CHAPTER V

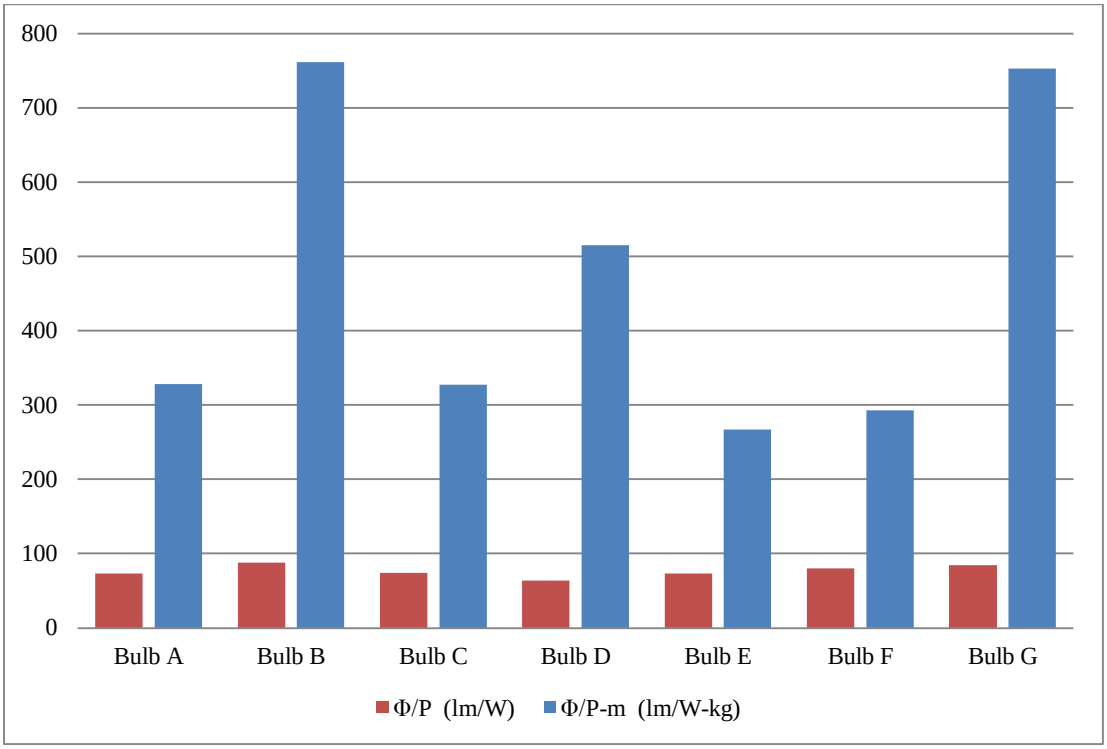

Figure 88: Variation of FOM_{LPW} and $FOM_{LPW,m}$ for various lamps

As presented in Figure 88, bulb-B has the highest luminous efficacy. Bulb-B's high performance is due to its efficacy of electrical and optical components, while bulb-G with the second highest luminous efficacy has the lowest maximum heat sink temperature, which is an indicator for a low junction temperature. This emphasizes the importance of power-lumen relation despite the thermal side. Bulb-F with higher input power and higher heat sink temperature has a higher luminous efficacy compared to bulb-E, which also indicates that the thermal performance alone is not adequate for a high luminous efficacy. Bulb-B has the best performance again based on mass. Bulb-G with the lowest weight has a very good luminous performance again based on $FOM_{LPW,m}$.

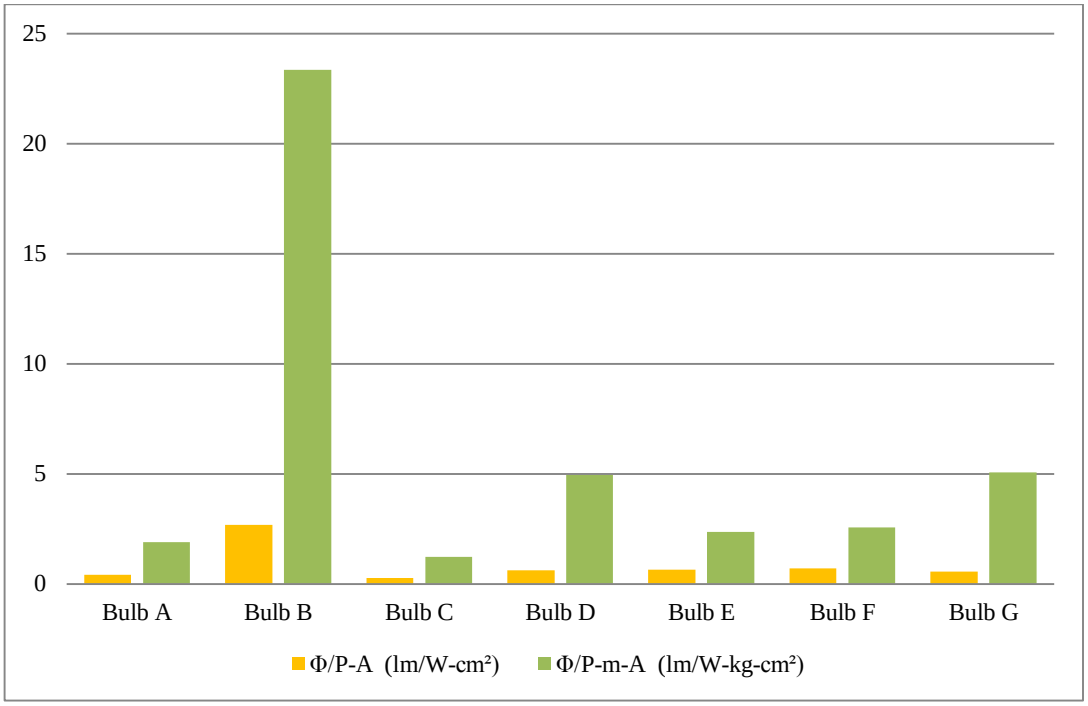

Figure 89: Variation of $FOM_{LPW,A}$ and $FOM_{LPW,m,A}$ for various lamps

As seen in Figure 89, bulb-B has the highest luminous performance based on surface area. Results show that bulb-G and bulb-D are advantageous based on mass and surface area. Bulb-B has by far the best performance due to $FOM_{LPW,m,A}$, since it has the highest luminous efficacy with the smallest heat sink and very low weight.

Finally, a new opto-thermal performance indicator is produced offering how much heat sink temperature rises per lumen (see Figure 90). Additional FOMs are also produced by multiplying opto-thermal resistance with mass (see Figure 90), surface area (see Figure 91) to bring various parameters together that need to be small against luminous flux for a high performance. Final FOM (see Figure 91) is the product of opto-thermal resistance, mass and surface area.

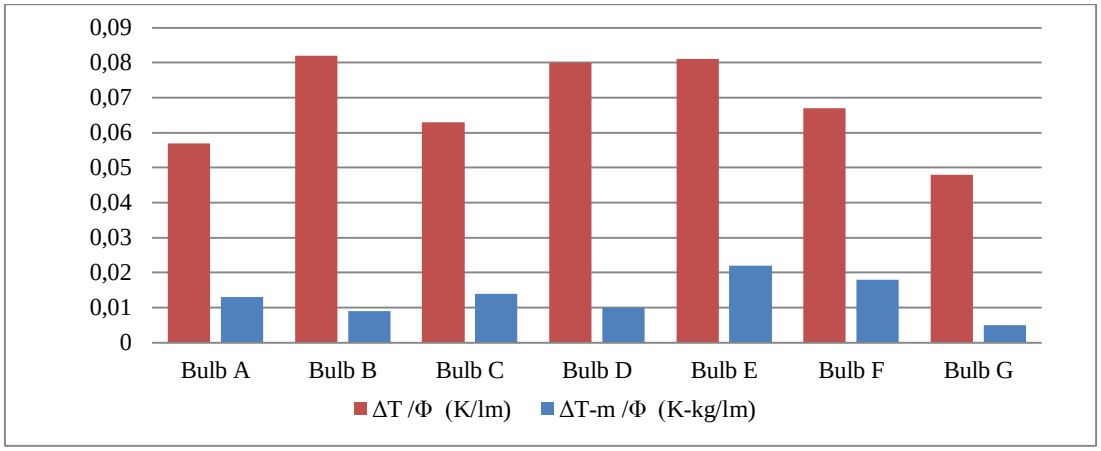

Figure 90: Variation of $FOM_{T,L}$ and $FOM_{T,m,L}$ for various lamps

Figure 90 shows that bulb-G has the best result based on $FOM_{T,L}$ due to its high luminous flux for low temperature rise. Bulb-A and bulb-C have satisfactory opto-thermal performances, which are the examples for the combination of smart optical design and effective cooling. Bulb-F with higher input power has a higher opto-thermal performance compared to bulb-E. Bulb-G's very good performance based on mass is due to its very low weight beside its low opto-thermal resistance. Bulbs B and D have good results based on $FOM_{T,m,L,}$ despite the fact that they have high opto-thermal resistances.

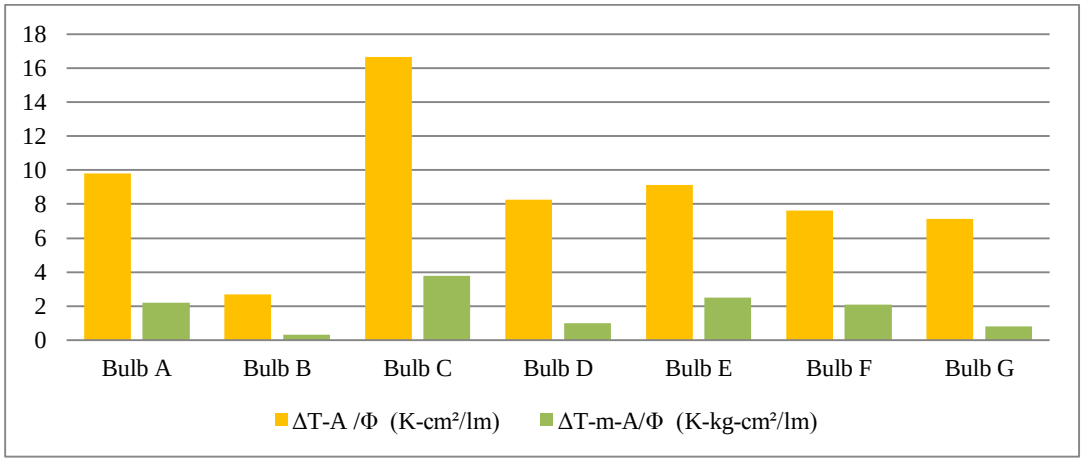

Figure 91: Variation of $FOM_{T,A,L}$ and $FOM_{T,m,A,L}$ for various lamps

Figure 91 indicates that bulb B has the lowest opto-thermal resistance based on surface area. Bulb-C has the poorest performance based on $FOM_{T,A,L}$. Results show that bulb-B has the highest opto-thermal performance for its product with mass and surface area. Extra ordinary performance of bulb-B is due to light-weight and small heat sink. Low opto-thermal resistance, small and light-weight heat sinks make bulb-G and bulb-D other advantageous products from the view of combined parameters. Bulb-C has the highest combined opto-thermal resistance due to large surface area and weight.

These newly proposed FOMs help to analyze as many complex aspects together as possible. But some points are not taken into account. Optical consideration includes only the luminous flux, not the light quality parameters like CCT and CRI. Bulb-G has the highest CCT, despite the fact that it has satisfying results for the rest of the primary concerns of vendors and consumers. Bulb-B with very high efficacy and low combined resistances has very good results; although it has the highest thermal resistance, which normally compromises reliability and lifetime. However, bulb-B is supposed to have a very long lifetime according to the information provided by manufacturer. It can be explained with the high quality of driver electronics and LEDs. Intricate surface area of heat sink is not desired by vendors in common but it does not directly mean that this will bring unacceptable time increase or price jump for the production. It is also possible to make this advantageous, when the lighting manufacturers have access for the development of the production technology. Evaluation based on surface area can be generalized for most of the current lamps as bulb-C, since expanding surface area made its structure very complex. However the structure of prototype with very large surface areas is not complicated thanks to new approach. It can be also easily manufactured and assembled, as experienced by preparing prototype. While these FOMs provide a tool to compare various design options, manufacturing and cost of the thermal solution should be considered together.

CHAPTER V

FOMs provide a good general view from many aspects. Some or all of them can be case-based used for a detailed analysis and comparison. It should be remarked that the evaluation method is not only based on cooling approaches or heat sink performances of lamps. In this study total system performances are presented, which is also affected by LED packages, driver electronics, optical components, other thermal components and different operational conditions. For a plain performance evaluation of various design approaches of heat sinks, thermal and optical analysis of lamps can be computationally performed based on CAD models under same conditions that may affect above mentioned factors in future studies.

In this study, a number of FOMs based on thermal resistance, luminous efficacy and newly proposed opto-thermal resistance are presented to offer a collective interpretation of LED lamps. This is crucial to understand the interaction of design variables. It gives researchers an opportunity to analyze the system on desired performance points and evaluate the system in a restricted area that has to be improved. Developed FOMs provide valuable information not only for engineers but also for vendors and consumers to understand LED lamps. While those proposed FOMs carry some insight, they can certainly be expanded by incorporating other performance metrics and, they can be improved to find the best-representing parameters for SSL products.

CHAPTER VI

CONCLUSIONS AND FUTURE WORK

In this study, current optical and thermal, as well as overall system related technologies of A-line LED lighting systems were investigated. Thermal, optical, electrical, mass, size and structural limitations of current approaches were brought into view. Following conclusions were drawn as:

- While thermal performance is crucial for the LED products, large heat sinks or other cooling components with large weights reduce consumer acceptance.
- Generating maximum amount of lumens at the minimum input power and low junction temperature increases total system performance.
- Power-lumen efficiency isolated from temperature dependence is also crucial.
- Developing a novel heat sink with the lowest thermal resistance and with an optimized mass is the key for improving LED systems.
- Efficacy, mass, thermal performance, input power, and heat sink as the key component all impacts LED systems and combined FOMs will help designers and end users.
- Design and cooling approach of the system should not be fixed based on only one aspect; manufacturer's respective manufacturing capability and costs for individual components enable the combinations of primitive and high tech components.

A new solid state lighting system approach was proposed by analyzing the current systems. The proposed system presented a total system solution and enhancement on all performance metrics. In light of results obtained, following conclusions are drawn for the new approach:

- Surface area was expanded for a higher heat transfer area for natural convection and thermal radiation.
- Mass of the system was reduced.
- Many optical design options were presented for homogenous and wide-angle intensity distribution.
- High heat sink efficiency was provided by spreading generated heat on a large heat sink area and effective heat transfer within heat sink.
- Angular heat sink base and vertical fins were matched with natural convection flows. Heat sink structure enabled a well-organized and strong natural convection development.
- Effective cooling of electronic driver circuit was possible without being of secondary priority.
- High luminous fluxes and LPWs were possible due to the extended thermal limitations.

Only considerable point was the high values for FOMs based on surface area. Opportunity of expanding the surface is already referred as an advantage for the new approach, since size limitations of A-line SSL systems do not allow high values for surface area. According to experimental observations in this study, expanding surface area of current approaches made the system structure more complicated. This proposition was produced based on the experimental analysis of current systems. However large surface area of new approach did not bring a considerable complexity in heat sink structure. Since it is a completely different system approach than current approaches, evolution of new approach based on larger surface area may not be seen as a disadvantage.

CHAPTER VI

Despite the obtained multi-aspect high performance of total system solution approach, there are still some areas, which can be further studied and improved. Some of future study areas are as follow:

- Optical design can present wider options for luminous intensity distribution by using two or more base angles for light engine.
- Dome can be subdivided in smaller pieces for a better match between fins and natural convection flow direction.
- Integration of a diffuser can be studied instead of using a transparent dome.
- Dome can be coated with phosphor for a better that management, which will prevent hot spots and provide more options for optical design.
- Thermal integration of heat sink with electronic driver circuit and light engine can be studied including advanced TIMs and mounting methods.

CHAPTER VII

REFERENCES

[1] http://www.superiorlighting.com/LED_Lamp_Components_Explained_s/2476.htm

[2] http://www.cree.com/Lighting/Products/Indoor/Lamps/A21-Series

[3] http://www.cree.com/Lighting/Products/Indoor/Lamps/MR16-Series

[4] http://www.illustralighting.com/media/catalog/product/cache/1/image/9df78eab33525d08d6e5fb8d27136e95/p/a/par38_xbd_h_1.jpg

[5] ANSI C78.20-2003, Revision of ANSI C78.20-1995, American National Standards Institute

[6] Arik M, Becker C, Weaver S, Petroski J, "Thermal Management of LEDs: Package to System," Third International Conference on Solid State Lighting, SPIE, Bellingham, WA, 2004.

[7] Changa MH, Das D, Varde PV, Pecht M, "Light emitting diodes reliability review," Microelectronics Reliability, Volume 52, Issue 5, Pages 762-782, May 2012.

[8] You JP, He Y, Shi FG, "Thermal Management of High Power LEDs: Impact of Die Attach Materials," Microsystems, Packaging, Assembly and Circuits Technology, IMPACT 2007, Taipei, 1-3 Oct. 2007.

[9] Petroski J, "Spacing of high-brightness LEDs on metal substrate PCB's for proper thermal performance," Thermal and Thermomechanical Phenomena in Electronic Systems, GELcore, Valley View, OH, USA, 2004.

[10] Fan A, Bonner R, Sharratt S, Ju YS, "An innovative passive cooling method for high performance light-emitting diodes," Semiconductor Thermal Measurement and Management Symposium, Pages 319-324, San Jose, CA, 18-22 March 2012.

[11] Inan MN, Arik M, "A multi-functional design approach and proposed figure of merits for solid state lighting systems," *Journal of Solid State Lighting* 2014, **1**:8

CHAPTER VII

[12] Alvin C, Chu W, Cheng C, Teng J, "Thermal Analysis of Extruded Aluminum Fin Heat Sink for LED Cooling Application," International Microsystems Packaging Assembly and Circuits Technology, Taipei, October 2011.

[13] Sapia C, Sozio G, "CFD transient model of the buoyancy heat transfer for a heat sink: Effects of geometry rotation," 18th International Workshop on Thermal Investigations of ICs and Systems, Budapest, 25-27 Sept. 2012.

[14] Dogruoz MB, Arik M, "On the Conduction and Convection Heat Transfer from Lightweight Advanced Heat Sinks," IEEE Transactions on Components and Packaging Technologies, Volume 2, 33rd edition, June 2010.

[15] B. Vermeersch, Mey GD, Wójcik M, Pilarski J, Lasota M, Banaszczyk J, Napieralski A, Paepe MD, "Chimney effect on natural convection cooling of electronic components," Journal of Electronic Packaging - J ELECTRON PACKAGING 01/2009; 131(1), DOI: 10.1115/1.3068307.

[16] Ishizuka M, Hatakeyama T, Nakagawa S, Kitamura Y, Funawatashi Y, "Chimney effect on natural air cooling of electronic equipment under inclination," ThETA 3, Pages 77-83, Cairo, 19-22 Dec. 2010

[17] Ishizuka M, Nakagawa S, "Study on the natural air cooling design of electronic equipment casings: Effects of the height and size of outlet vent on the flow resistance," ITHERM 2008, Orlando, FL, 28-31 May 2008.

[18] Klein, B, "FEM Grundlagen und Anwendungen der Finite-Element-Methode im Maschinen- und Fahrzeugbau," Vieweg+Teubner Verlag, June 2007.

[19] www.smart-fem.de

[20] Tu J, Yeoh GH, Liu C, "Computational Fluid Dynamics: A Practical Approach," Butterworth-Heinemann, 2008.

[21] Lecheler S, "Numerische Strömungsberechnung – Schneller Einstiegdurch ausführliche praxisrelevante Beispiele," Vieweg+Teubner Verlag, November 2008.

[22] Taylor AEF, "Illumination Fundamentals," Rensselaer Polytechnic Institute, 2000.

CHAPTER VII

[23] http://optics.synopsys.com/lighttools/

[24] ENERGY STAR Program Requirements for Lamps, "Elevated Temperature Life Test Method," Revision in January 2013

[25] http://www.flir.com/cs/emea/en/view/?id=42577

[26] http://www.omega.com/temperature/Z/pdf/z207.pdf

[27] FLIR IR camera manual, 090901 SC5000 Datasheet

[28] http://www.sphereoptics.de/de/lichtmesssysteme/docs/LargeSphere_photopic_Systems.pdf

[29] Illuminating Engineering Society, "IES LM-79-08, Approved Method: Electrical and photometric Measurements of Solid-State Lighting Products," December 31, 2007.

[30] http://www.lmt-berlin.de/en/gov1900.html

[31] Liu S, Luo X, "LED Packaging for Lighting Applications: Design, Manufacturing, and Testing," Wiley, 1 edition, July 2011.

[32] Driel WD, Fan XJ, "Solid State Lighting Reliability: Components to Systems," Springer, 2013 edition, September 2012.

[33] Karsli K, Arik M, "Effect of Optical Design on the Thermal Management for the Smart TV Backlight Systems," Electronic Components and Technology Conference (ECTC), 2014 IEEE 64th, Orlando, FL, 27-30 May 2014.

[34] Khosroshahi FS, Tufekci CS, Arik M, "A Computational and Experimental Study on a Harsh Environment LED System for Vehicle Exterior Lighting Applications," Thermal and Thermomechanical Phenomena in Electronic Systems (ITherm), Orlando, FL, 27-30 May 2014.